Summer 8-2018

Fabrication and Characterization of a Magnetohydrodynamic Micropump from Polydimethylsiloxane (PDMS)

Rachel K. Weber
Rose-Hulman Institute of Technology

Fabrication and Characterization of a Magnetohydrodynamic Micropump from Polydimethylsiloxane (PDMS)

A Thesis

Submitted to the Faculty

of

Rose-Hulman Institute of Technology

by

Rachel K. Weber

In Partial Fulfillment of the Requirements for the Degree

of

Master of Science in Chemical Engineering

August 2018

ROSE-HULMAN INSTITUTE OF TECHNOLOGY

Final Examination Report

Rachel Weber — Name

Chemical Engineering — Graduate Major

Thesis Title: Fabrication and Characterization of a Magnetohydrodynamic Micropump from PDMS

DATE OF EXAM: August 8, 2018

EXAMINATION COMMITTEE:

	Thesis Advisory Committee	Department
Thesis Advisor:	Daniel Anastasio	CHE
	Kimberly Henthorn	CHE
	Daniel Morris	CHEM

PASSED X **FAILED** _____

ABSTRACT

Weber, Rachel K.

M.S.Ch.E.

Rose-Hulman Institute of Technology

August 2018

Fabrication and Characterization of a Magnetohydrodynamic Micropump from Polydimethylsiloxane (PDMS)

Thesis Advisor: Dr. Daniel Anastasio

Microfluidics is a growing area of study in recent years, particularly for lab-on-a-chip applications. Fluids must oftentimes be transported from one location on the chip to another. This study focuses on the fabrication and characterization of a magnetohydrodynamic micropump. The device was fabricated in the Rose-Hulman Institute of Technology MiNDS facility, and consisted of a PDMS channel and titanium electrodes supported on a glass slide with a permanent magnet. An Arduino microcontroller capable of pulse width modulation (PWM) was used to control the electrical potential. An electrode design that spanned the full length of the channel was successful in driving fluid motion. Erioglaucine disodium salt blue dye was used to track the fluid motion through the channel, and appeared to have a greater impact on the apparent fluid velocity than sodium chloride. Of the PWM duty cycles tested, 75% had the highest apparent fluid velocity. The titanium that contacted the fluid anodized, indicating it is best suited for disposable applications.

Keywords: Chemical engineering, microfluidics, MEMS, magnetohydrodynamic micropumping

ACKNOWLEDGMENTS

I would first like to thank my advisor, Dr. Daniel Anastasio, without whose guidance this project would never have gotten off the ground. I would also like to thank the rest of my advisory committee, Dr. Kim Henthorn and Dr. Daniel Morris, for their support in answering all of my questions throughout this process.

I would particularly like to thank Brian Fair, Cleanroom Facility Manager and Instrumentation Technician, and Frank Cunning, Technician in the Department of Chemical Engineering, for their help in fabricating the device and using the lab space.

Finally, I would like to thank my family and friends, whose love and support is truly invaluable.

TABLE OF CONTENTS

Contents

LIST OF FIGURES

1. INTRODUCTION

1.1 Background

Microfluidics is a broad category, encompassing any fluidic device with at least one dimension on the micron scale (1-999 μm). Microfluidic devices have the potential to serve as chemical reactors or perform other fluidic tasks while consuming small volumes of reactants. Small volumes are ideal when working with potentially dangerous and/or expensive chemicals for reducing risk and cost. Reducing the size of the device can also improve the portability of the device. There are many applications of microfluidic devices, including research in cell biology, micro fuel cells, drug screening, and glucose tests [1]. One of the most prominent and promising applications of microfluidics is the idea of lab-on-a-chip technology. Lab-on-a-chip refers to a self-contained microfluidic device for chemical testing or reactions. In some cases, lab-on-a-chip devices, such as the one shown in Figure 1.1.1, are fabricated through 3D printing and are used as reactionware [2]. Another common fabrication technique is lithography.

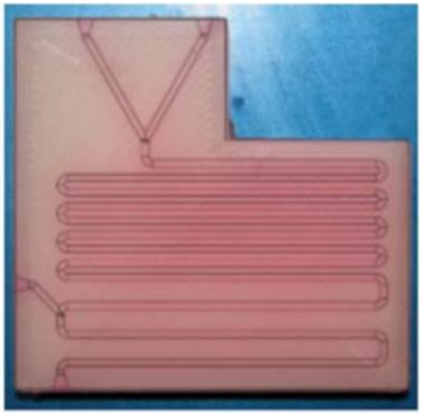

Figure 1.1.1: A 3D printed microfluidic device to be used as reactionware. The channels are filled with a methanol solution of Rhodamine B dye for visibility [2].

Often, however, lab-on-a-chip devices are fabricated for medical applications, as multiple tests can be fabricated on one device [1]. An example lab-on-a-chip device is shown in Figure 1.1.2. The small size and portability allow for point of care testing, low consumption of chemical reactants, low required sample size, high throughput, and fast response times [3]. Sample collection from patients can require invasive procedures, and removing excess blood or other materials from the body can cause additional problems in the patient. Reducing the required sample size for testing has the potential to reduce the impact of sample collection on the patient. For example, the lab-on-a-chip technology could take tests that normally require a blood draw and develop tests that only require a finger prick. Faster times for results are also important. Instead of shipping samples to a specialty lab and waiting days or weeks for results, point of care tests can deliver results in minutes or hours.

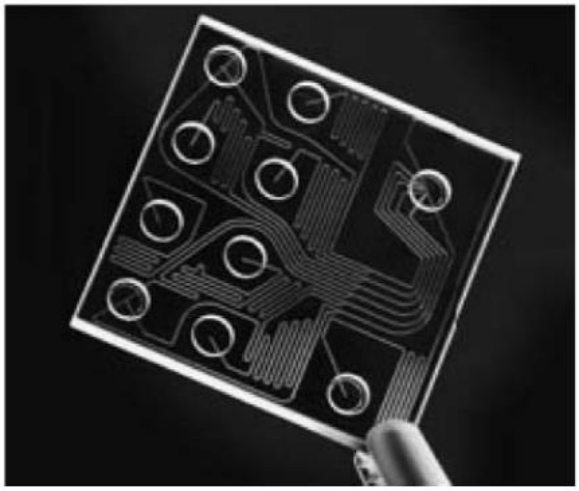

Figure 1.1.2: An example of a droplet-based lab-on-a-chip device [3].

Often, lab-on-a-chip microfluidic devices require that fluids be transported through channels from one location on the chip to another. Fluid motion is required to initiate mixing and/or reactions. This movement requires some element of driving force. There are many types of micropumps available to deliver this driving force. Generally, micropumps fall into two broad categories: mechanical pumps and non-mechanical pumps.

One type of mechanical micropump is a rotary pump [4]. Rotary pumps use a gear operated by an electric motor, and collect fluid between the teeth of the gear to transfer the fluid from the inlet to the outlet [4]. An example of a rotary micropump is shown in Figure 1.1.3.

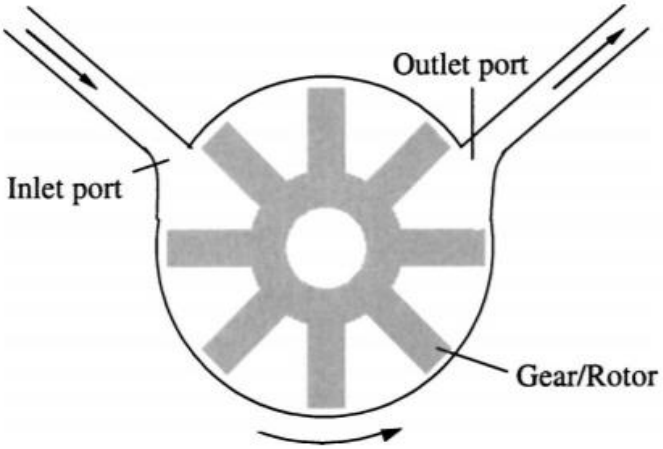

Figure 1.1.3: A schematic of a rotary micropump [4].

Another mechanical micropump is a vibrating diaphragm pump, which has unidirectional valves at the inlet and outlet of a chamber to control the direction of fluid flow [4]. The diaphragm is pulled away from the chamber to reduce the internal pressure and accept incoming fluid. The diaphragm is then pushed into the chamber to increase the internal pressure and force fluid out the other side [4]. The operation of a vibrating diaphragm micropump is depicted in Figure 1.1.4.

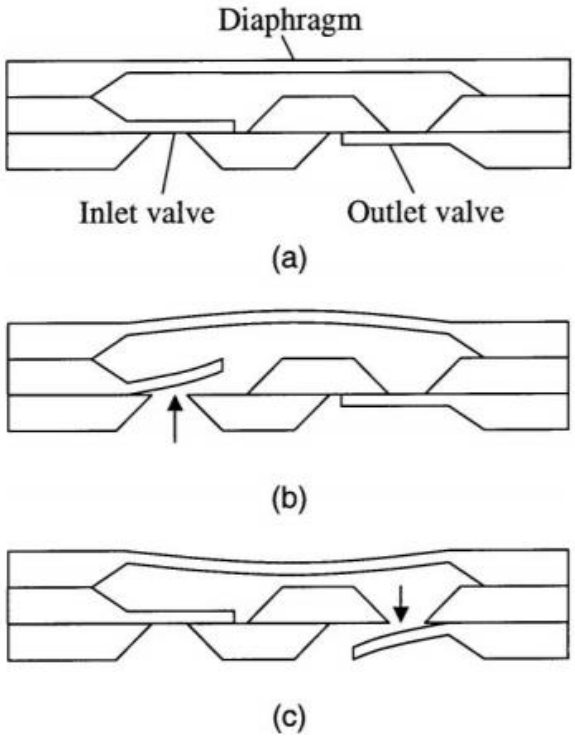

Figure 1.1.4: Operation of a vibrating diaphragm micropump. (a) Schematic of the micropump (b) The micropump drawing fluid in (c) The micropump forcing fluid out [4].

Peristaltic pumps, the final type of mechanical micropump, are similar to vibrating diaphragm pumps in that both use actuating diaphragms. However, peristaltic pumps do not use valves to control the direction of flow. Instead, peristaltic pumps consist of three diaphragms in series. The first contracts, forcing fluid into the second and closing the inlet. The second and third contract in sequence, forcing fluid to flow. The first diaphragm remains closed, preventing backflow [4]. The operation of a peristaltic micropump is shown in Figure 1.1.5.

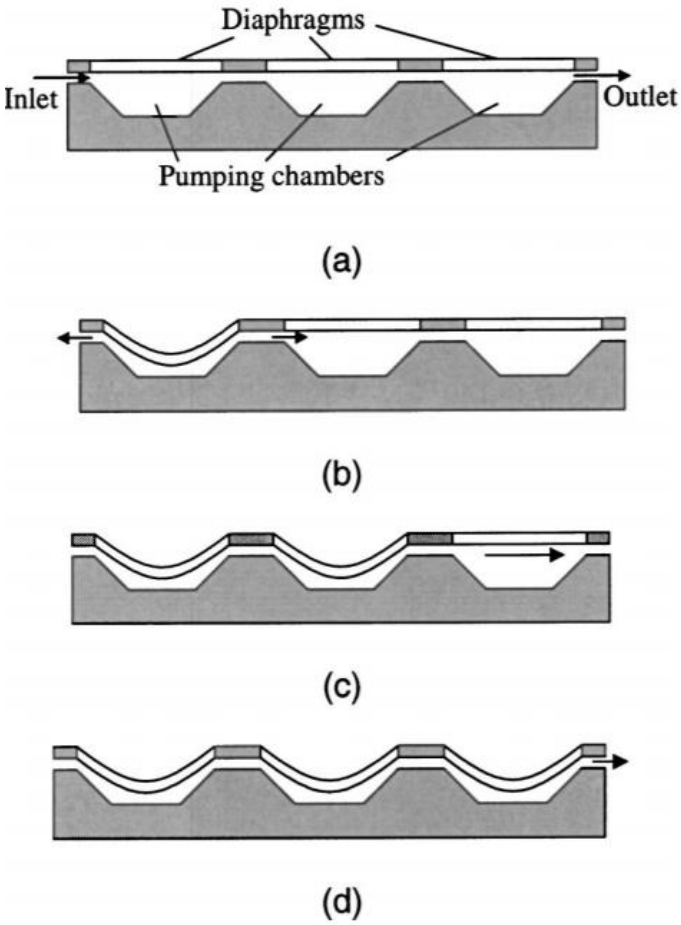

Figure 1.1.5: Operation of a peristaltic micropump. (a) Schematic of the micropump (b) Contraction of the first diaphragm, forcing fluid into the second and third chambers (c) Contraction of the second diaphragm, forcing fluid into the third. The first remains closed, preventing backflow (d) Contraction of the third diaphragm, forcing fluid flow [4].

Vibrating diaphragm pumps and peristaltic pumps can use a variety of different actuation methods. One actuation method is an electrostatic method, where an applied voltage induces charges on plates, creating an attractive force [5]. In the piezoelectric actuation method, an electrical voltage causes a mechanical stress [5]. With the thermo-pneumatic actuation technique, an air-filled chamber is heated and cooled, causing pressure changes and driving flow [5]. Shape memory alloy actuation involves heating and cooling between two solid phases, each of which has a slightly different shape [5]. Bimetallic actuators are fabricated from two metals with different coefficients of thermal expansion. When heated, the deformation is forced in a single direction

based on the geometry of the metals and the coefficients of thermal expansion [5]. In ion conductive polymer film actuation, charged ions in the polymer film are attracted to electrically charged plates. Alternating current is used to move opposite polymer films [5]. With electromagnetic actuation, a permanent magnet and an electric coil are used to move a solenoid plunger [5]. Magnetic actuation can be achieved by embedding magnetic particles in the flexible diaphragm material and applying a magnetic field [6]. Irreversible actuators can be used in disposable applications, and can be driven by swelling of ionic polymers or thermal expansion [6].

In addition to the mechanical micropumping techniques available, there are also several non-mechanical micropumping techniques. One such non-mechanical pump type is an electrohydrodynamic (EHD) pump. EHD pumps use "electrostatic forces acting on dielectric liquids to generate flow" [6]. There are multiple techniques to place the required ions in solution, and each are shown in Figure 1.1.6. Induction-type EHD pumps use a fluid with a non-uniform conductivity or permittivity coupled with an alternating voltage to induce charges [6]. Injection-type EHD pumps have electrochemical reactions at the electrodes which put free ions into the fluid [6]. Polarization-type EHD pumps use a non-homogeneous electric field through the fluid to create dipoles [6].

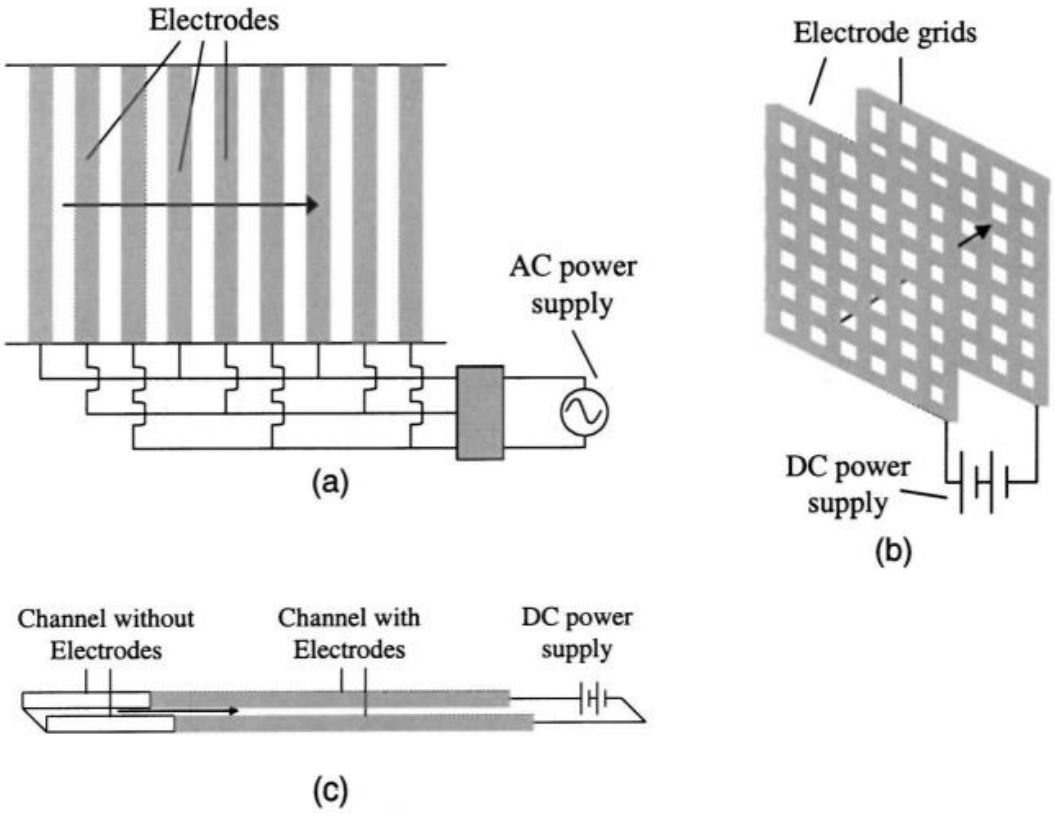

Figure 1.1.6: Diagrams of (a) induction-type, (b) injection-type, and (c) polarization-type EHD micropumps [4].

Electroosmotic (DC or AC) pumps take advantage of the electric double layer formed at the surface of the channel, and an electrical potential induces fluid motion [4-6]. A schematic is shown in Figure 1.1.6.

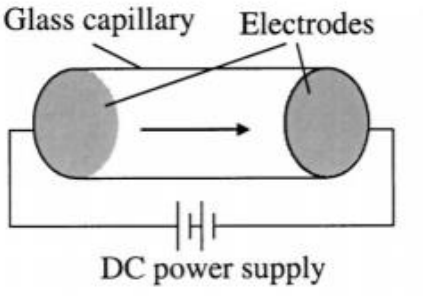

Figure 1.1.7: Schematic of an electroosmotic pump [4].

Magnetohydrodynamic (MHD) micropumps operate through the Lorentz force, where an electric and a magnetic field are coupled. Electrowetting pumps use metals contacted with

electrolytic solutions, where an electrical potential is used to change the wettability of the surface and motion is driven by surface tension [5]. A schematic of an electrowetting micropump is shown in Figure 1.1.8.

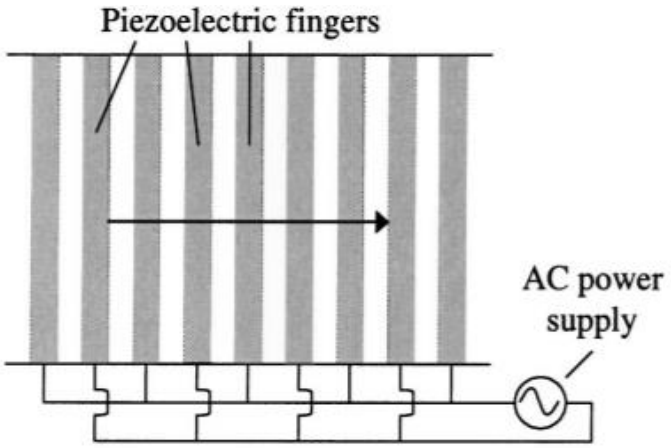

Figure 1.1.8: A schematic of an electrowetting micropump [4].

Bubble type micropumps operate through the periodic expansion and collapse of bubbles generated through a voltage input [5]. Electrochemical pumps use electrolysis to break down water and form gaseous species that drive flow [5]. Optoelectrostatic microvortex pumps operate in the presence of an AC field around the focal point of a laser beam to generate fluid flow [6]. A summary of the discussed micropumping techniques is available in Table 1.1.1.

Table 1.1.1: Summary of micropumping techniques.

Mechanical Micropumping Techniques	Non-Mechanical Micropumping Techniques

• Rotary
• Vibrating diaphragm
  ○ Electrostatic
  ○ Piezoelectric
  ○ Thermo-pneumatic
  ○ Shape memory alloy
  ○ Bimetallic
  ○ Ion conductive polymer film
  ○ Electromagnetic
  ○ Magnetic
  ○ Irreversible
• Peristaltic
	• Electrohydrodynamic
	  ○ Induction-type
	  ○ Injection-type
	  ○ Polarization-type
	• Electroosmotic
	• Magnetohydrodynamic
	• Electrowetting
	• Bubble-type

Each microscale pumping technique has advantages and limitations, and selections are made based on the particular requirements of a given system. One of the biggest challenges in micropumping is the microscale fabrication. Mechanical micropumping techniques in particular require microscale moving parts, which, though feasible, are challenging and costly to fabricate, and typically involve techniques such as thin film deposition and plasma etching [1]. Non-mechanical micropumping techniques have been of particular interest, since they do not require moving parts, simplifying fabrication and improving yield.

One technique of particular interest is MHD micropumping. MHD pumps use an electric current perpendicular to a magnetic field to drive fluid motion [7]. An electrically conductive fluid will then flow perpendicular to both fields, as shown in Figure 1.1.3. Macro scale MHD pumps have a long history of being used industrially to move liquid metals [8-12], but MHD technology also has applications in microfluidic pumping of electrolytic solutions or liquid metals. Micro-scale MHD pumps require a channel, a magnetic field source, and an electrical current source.

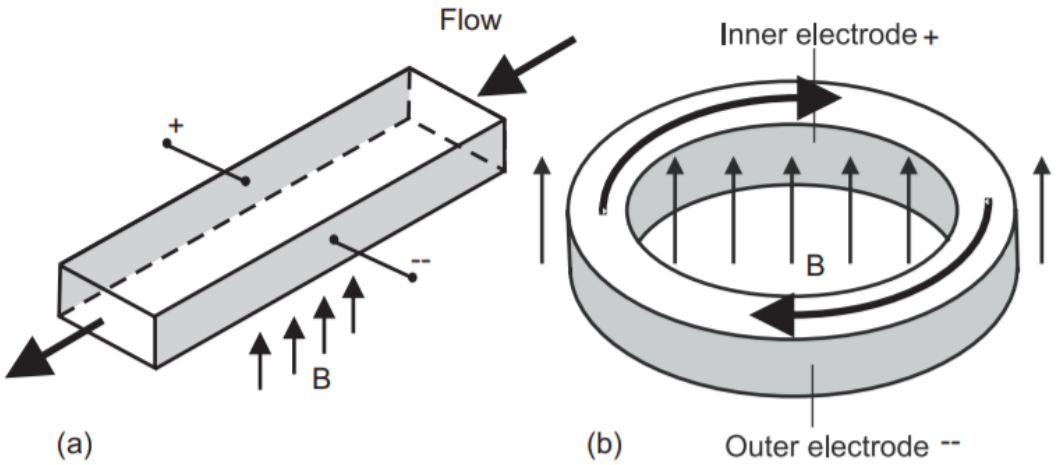

Figure 1.1.9: Two configurations of MHD micropumps: (a) straight channel (b) annular channel. The small arrows labeled 'B' indicate the direction of the magnetic field. The large arrows indicate the direction of fluid flow [7].

1.2 Previous Research

Previous research in MHD micropumping can largely be categorized by the substrate material chosen for the pump and the intended application of the pump. Much of the current research has been done in MHD micropumps fabricated on silicon wafers for use in lab-on-a-chip applications, as micromachining techniques for silicon are well established. Early research on silicon substrates focused on proof of concept [13] and configurations for complex routing in lab-on-a-chip applications, creating switches [14]. An illustration of the configuration for one early MHD micropump is shown in Figure 1.2.1. The schematic for MHD micropumps as switches is shown in Figure 1.2.2.

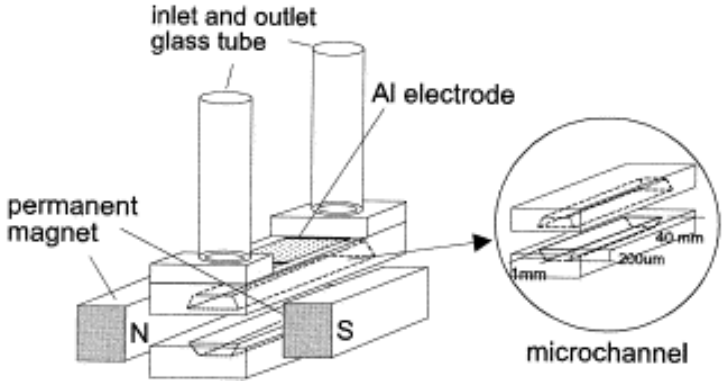

Figure 1.2.1: Illustrated depiction of an early MHD micropump [13]. Two silicon wafers were aligned to form the channel for fluid flow.

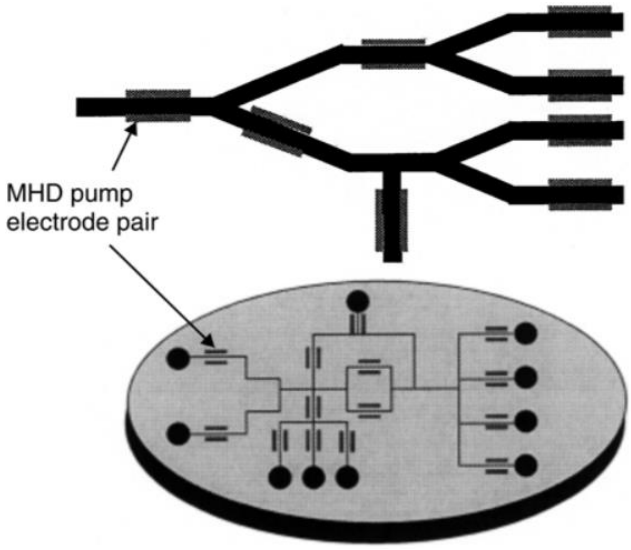

Figure 1.2.2: Schematic of a lab-on-a-chip device with MHD micropumps as switches [14].

Early MHD micropump configurations, such as the one shown in Figure 1.2.1, had electrodes on the top and bottom surfaces to create the electric field. This required fabrication with two silicon wafers bonded together with epoxy [13], as shown in Figure 1.2.3. Each silicon wafer formed half of the channel. Each wafer was etched; then the electrodes were deposited and patterned. The final step was alignment of the two silicon wafers and bonding to form the full channel.

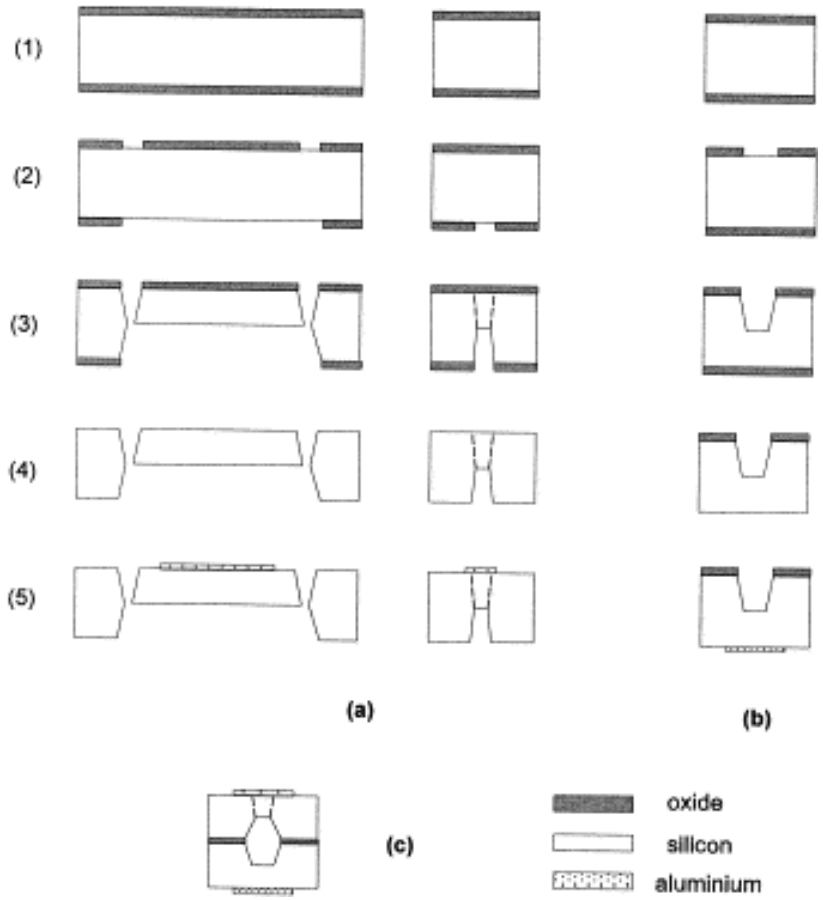

Figure 1.2.3: Process flow diagram of an early MHD micropump, shown in Figure 1.2.1. This process flow requires two similarly machined silicon wafers to be bonded together with epoxy [13].

More recent research in silicon-based MHD micropumps has focused on mathematical modeling of the devices, both for thermal effects [15] and for slip conditions [16]. Research into MHD micropumps with side wall electrodes has been done as well [17-19]. Sidewall electrodes,

as shown in Figure 1.2.4, allow for fabrication with a single silicon wafer. Fabricating with two wafers requires an alignment step to form the complete channel. Alignment on the microscale is challenging, and misalignment results in a non-functioning device. A single wafer fabrication method has the advantage of eliminating the final alignment step. Other applications of silicon-based MHD micropumps have been researched as well, such as liquid metal micro-cooling systems [20].

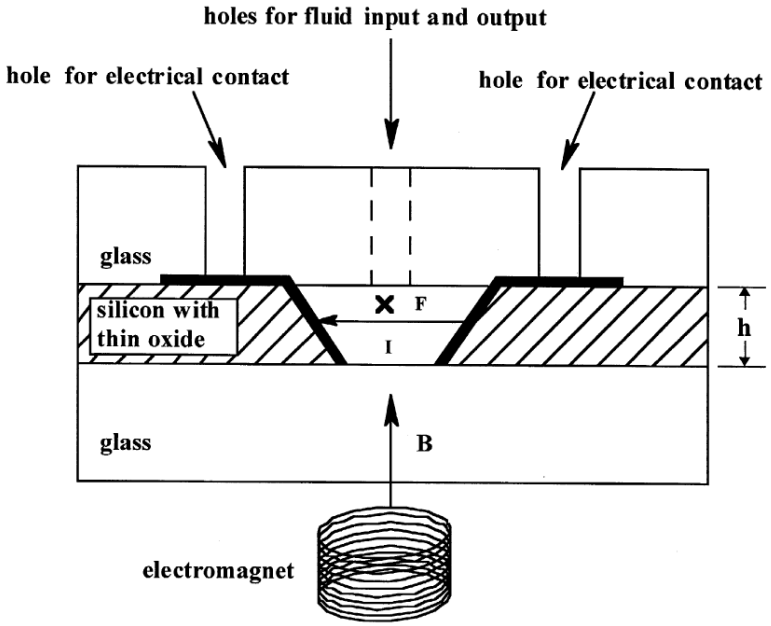

Figure 1.2.4: A cross-section of an MHD micropump with sidewall electrodes [17].

MHD micropumps have been fabricated on non-silicon substrates as well. Polysulfone [21], ceramic tapes [22], pyrex [23], photosensitive glass [24], low temperature co-fired ceramic (LTCC) [25], and polydimethylsiloxane (PDMS) with gold electrodes [26] have all been used as substrates for MHD micropumps. Using alternative materials to fabricate the micropump can allow the device to handle chemicals that react with silicon, and to employ fabrication techniques that are less costly.

Silicon is by far the most commonly used substrate for fabricating MHD micropumps. However, fabricating on silicon requires costly equipment and time-consuming processing. A

single step in the fabrication process can take several hours. In contrast, PDMS only requires micromachining equipment for the development of a mold [27]. Once the mold is made, it can be used repeatedly to make multiple devices, saving time and costs [27]. The relatively low cost of PDMS makes it ideal for disposable device fabrication, as the small channel size prevents sufficient cleaning to allow for multiple uses in medical applications.

One limitation faced by MHD micropumps is electrolysis and bubble formation. Electrolysis is the breakdown of water into hydrogen and oxygen in the presence of an electrical potential. The reactions at the cathode are [21]

$$2H_2O + 2e^- \rightarrow 2OH^- + H_{2(g)} \quad (1.2.1)$$

The reactions that occur at the anode are [21]

$$2H_2O \rightarrow O_{2(g)} + 4H^+ + 4e^- \quad (1.2.2)$$

Bubbles formed within the channel can lift the fluid away from the electrode, preventing current from flowing between electrodes. Different techniques have been tried to control the electrolysis problem, such as bubble release chambers [21] and AC signals for the electrical signal and an electromagnet [17]. An AC signal switches which reactions are occurring at each location, preventing bubble formation. However, when a permanent magnet is used, an AC signal for the electrical component will drive fluid flow in alternating directions. Permanent magnets offer power savings over electromagnets and are not subject to electrical failures. An alternate solution to an AC signal must be devised to prevent electrolysis and bubble formation. Since electrolysis is caused when a DC voltage is constantly applied, it is possible that periodically turning the signal off could lessen its effects. A microcontroller, such as an Arduino, could be used to control the on/off pattern of a DC signal when coupled with a permanent magnet.

The Arduino is a microcontroller platform that is capable of outputting a DC signal at 5 V. However, it can also output a square wave. The magnitude of the square wave is 5 V and does not reverse, as in an AC signal. It merely turns the forward voltage on and off. The percentage of time the signal is high, or the duty cycle, is controllable with the code [28], as demonstrated in Figure 1.2.5. This capability is referred to as pulse width modulation (PWM) and is a potential solution to the electrolysis problem experienced by MHD micropumps without using an AC signal.

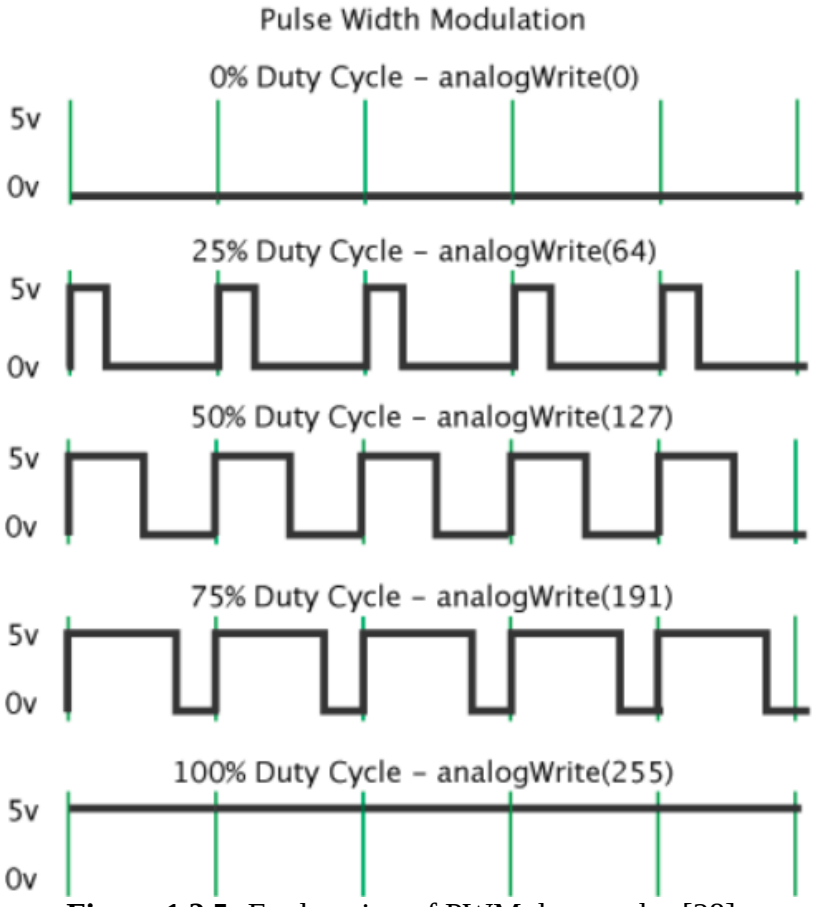

Figure 1.2.5: Explanation of PWM duty cycles [28].

2. THEORY

MHD pumps, both on a large scale and on a small scale, operate through the Lorentz force, which uses electric and magnetic fields to exert a force on a point charge. The Lorentz force operates on charged particles perpendicular to magnetic and electric fields or currents [18], as depicted in Figure 2.1. In an electrolytic solution, the Lorentz force acts on the ionic species. Momentum transfer then accounts for the bulk fluid motion.

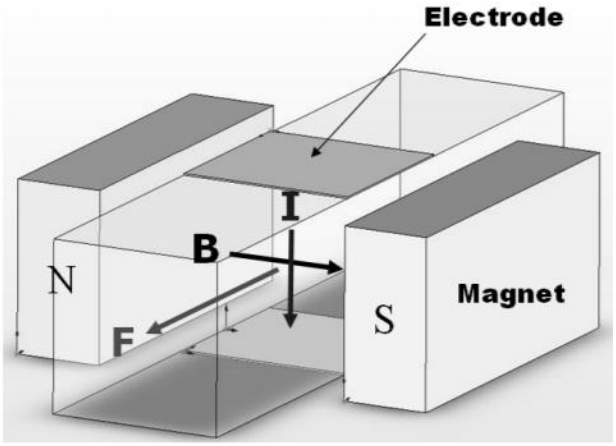

Figure 2.1: Visual representation of the Lorentz force. The current is represented by I, B is the magnetic field, and F is the Lorentz force [18].

The Lorentz force is calculated through the following equation [7]:

$$F_{Lorentz} = q(E + v \times B) \tag{2.1}$$

where q is the charge of a charged species, v is its velocity, E is the electric field, and B is the magnetic field. However, in the absence of an electric field, qv summed over a unit volume becomes the current density, J, and the equation simplifies to [7]

$$F_{Lorentz} = J \times B \tag{2.2}$$

Equation 2.2 is often reported as the governing equation [13, 18]. However, it is important to note that the current density simplification is only valid for electrically conducting fluids, such as electrolytic solutions and liquid metals [18].

To solve the fluid flow through the pump, the first step is to start with the continuity equation [29].

$$\frac{\partial \rho}{\partial t} + \underline{\nabla} \cdot (\rho \underline{v}) = 0 \tag{2.3}$$

The density is ρ, t is time, $\underline{\nabla}$ is the gradient, and $\underline{v}$ is the velocity. The underbars indicate vectors. Assuming that the liquid is incompressible, the continuity equation simplifies to the following.

$$\underline{\nabla} \cdot \underline{v} = 0 \tag{2.4}$$

The simplified continuity equation indicates that if the fluid decelerates in one direction, it must accelerate in another direction as a result of the incompressibility and steady-state operation, so there can be no accumulation.

The next step is to consider the conservation of momentum equation for Newtonian and Incompressible fluids, or the Navier-Stokes equation [29]

$$\rho \left(\frac{\partial \underline{v}}{\partial t} + \underline{v} \cdot \underline{\nabla}\, \underline{v} \right) = -\underline{\nabla} P + \rho \underline{g} + \mu \nabla^2 \underline{v} \tag{2.5}$$

where P is the pressure, $\underline{g}$ is gravity, and μ is the fluid viscosity. Assuming that the pump is oriented horizontally, the gravity term is zero. However, the additional Lorentz force, Equation 2.2, must be considered. Removing the gravity term and adding the Lorentz force results in the following equation [13]. Both gravity and the Lorentz force are per volume body forces, so the substitution requires no unit conversions. Though the Lorentz force only truly acts on the ionic species, the momentum transfer accounting for the bulk fluid motion is incorporated in the term.

$$\rho\left(\frac{\partial \underline{v}}{\partial t} + \underline{v} \cdot \underline{\nabla}\, \underline{v}\right) = -\underline{\nabla} P + \mu \nabla^2 \underline{v} + J \times B \tag{2.6}$$

The small size of the channel and low flowrates contribute to a low Reynolds number, defined as the ratio of inertial forces to viscous forces, shown below

$$Re = \frac{\rho v L}{\mu} \tag{2.7}$$

where L is the characteristic length particular to the geometry of the channel. The small size and flowrates, or low L and v, account for a low Reynolds number. The low Reynolds number means the flow is in the Stokes regime, also referred to as creeping flow. The cutoff for Stokes flow is Re < 0.1 [30]. Stokes flow refers to flow where the viscous forces are large compared to the inertial forces. In Stokes flow, the three terms on the right hand side of Equation 2.6 dominate [13].

$$0 = -\underline{\nabla} P + \mu \nabla^2 \underline{v} + J \times B \tag{2.8}$$

For the MHD micropump, Equation 2.8 is the governing equation [13]. In Stokes flow, effects from changing forces propagate instantaneously [31]. This means turning on the pump should result in instantaneous fluid motion. The major inhibitors to flow are viscosity and change in pressure, so flow can be improved by reducing the viscosity of the working fluid, reducing the friction, and ensuring the inlet and outlet are at the same height.

3. OBJECTIVES

The objectives of this work were to:

1. Fabricate and analyze an MHD micropump with a PDMS substrate for use in lab-on-a-chip applications. PDMS was chosen over silicon based on its comparatively low cost and ease of fabrication. It was expected that a PDMS substrate would function well for

the channel, as the substrate material does not impact the Lorentz force, and would be well suited to disposable applications. Medical devices require high levels of cleanliness, which are difficult to achieve in micro-scale geometries. A PDMS substrate offers a cheap way to fabricate the channel, and disposing after one use maintains the required level of cleanliness.

2. Study the impact of PWM and the duty cycle of the DC signal on the pumping rate and as a potential new solution to the electrolysis problem. It was expected that the duty cycle would reduce the impact of electrolysis on the flow rate. Electrolysis occurs when an electrical current is passed through water, and turning the current off should stop the reaction. By stopping the reaction, bubble formation was expected to reduce.
3. Analyze the impact of salt concentration on the pumping rate. Since the Lorentz force acts on charged species, it was expected that reducing the ion concentration would reduce the flow rate [17].
4. Fabricate with titanium as the electrode material, as titanium offers cost savings over gold. It was expected that using titanium would not impact the performance of the device, since it is also a good electrical conductor.

4. FABRICATION AND ANALYSIS: MATERIALS AND METHODS

An overall cross-section of the device that was fabricated is shown in Figure 4.1 as a reference.

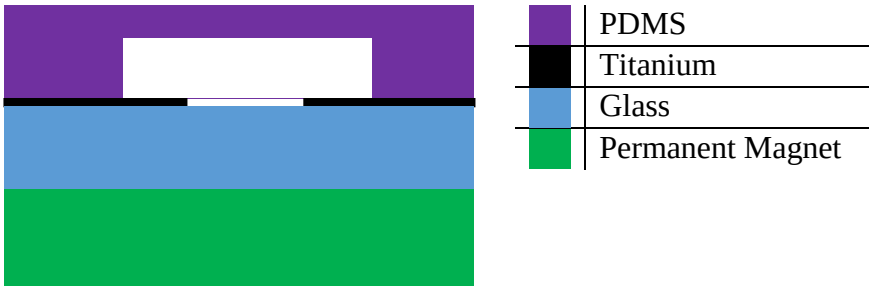

Figure 4.1: A cross-section of the MHD micropump.

4.1 Materials

The materials used to fabricate the device were as follows:

- 4-inch silicon wafer, p-type, crystal orientation: <100> (University Wafer, South Boston, MA)
- SU-8 negative photoresist (MicroChem, Westborough, MA)
- SU-8 developer, 1-methoxy-2-propyl acetate (MicroChem, Westborough, MA)
- Sylgard 184 elastomer, polydimethylsiloxane (PDMS), base and curing agent (Ellsworth, Germantown, WI)
- Glass slide
- Physical vapor deposition (PVD) titanium
- SPR3622 positive resist (MicroChem, Westborough, MA)
- SPR3622 developer (MicroChem, Westborough, MA)

The materials used to test the device were as follows:

- NaCl, Morton All-Purpose Natural Sea Salt
- Tartrazine (Sigma Aldrich, St. Louis, MO)
- Erioglaucine disodium salt (Sigma Aldrich, St. Louis, MO)
- Permanent magnet disk 40x20 mm, DIYMAG, 8.242 mT $\pm$ 0.004 mT

4.2 Fabrication of the Channel

4.2.1 Channel Fabrication Overview

Fabrication of the microfluidic flow channel and electrodes was performed in the Rose-Hulman Institute of Technology (RHIT) Micro-Nanoscale Device and Systems (MiNDS) facility. The channel was formed by casting a polymer over a mold. A clean four-inch silicon wafer was used as the base for the mold. Crystal orientation and doping were not expected to impact the performance. SU-8 negative photoresist was used to form the channel portion of the mold.

Photoresists are chemicals that interact with light, and are typically used in MEMS and semiconductor manufacturing processes to form patterns by exposing a thin layer of the chemical to a UV light through a mask, or a master with the desired pattern. There are two main types of photoresists, positive photoresist and negative photoresist. Negative photoresists crosslink when exposed to UV light, and positive photoresists become more soluble when exposed to UV light [32]. A developer is then used to remove the portions of the photoresist that are the most soluble and complete the pattern. In the case of negative photoresist, the portions that were not exposed to light are rinsed away [32]. SU-8 was selected over the available positive resist because it was experimentally determined to form thicker layers and was more mechanically stable. Since this photoresist is forming the mold for the channel, building a thick layer is critical to forming a sufficiently deep channel. The mold can potentially be used many times to form many channels, so mechanical stability is important to ensure the channel formed is uniform each time and the mold is not damaged in the process.

4.2.2 Mold Process Flow

The process flow for fabricating the mold is shown below. The mold process flow is summarized in Figure 4.2.2.1.

1. Start with a clean, bare silicon wafer.
2. Pre-bake for 5 minutes at 65ºC.
3. Spin SU-8 negative photoresist on the wafer.
4. Soft bake for 5 minutes at 95ºC.
5. Expose for 21 seconds of hard contact through the channel mask.
6. Post-exposure bake for 1 minute at 65 ºC and 1 minute at 95ºC.
7. Develop, removing excess resist.
8. Hard bake for 5 minutes at 160ºC.
9. Repeat steps 3-8 for a total of four layers.

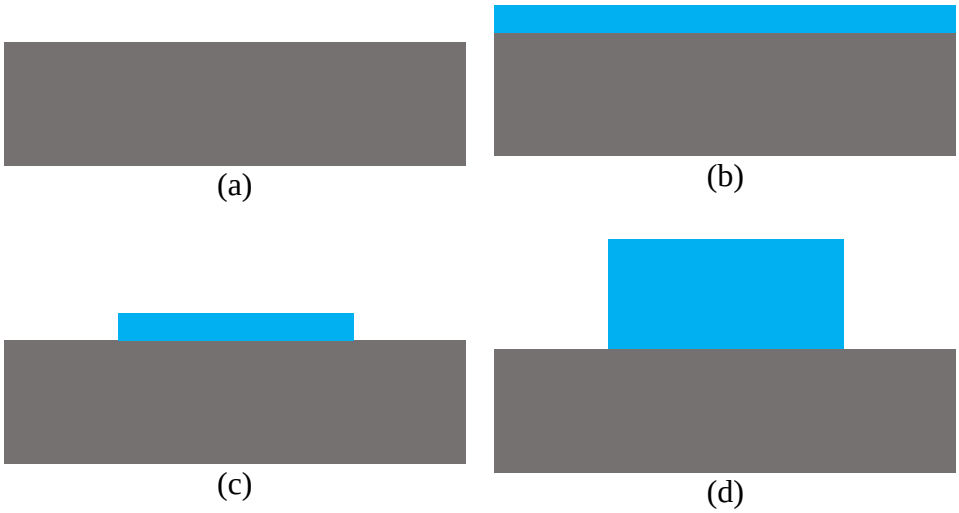

Figure 4.2.2.1: Illustrations of the process flow for fabricating the mold. Grey is the silicon and blue is the SU-8 negative photoresist. (a) Clean, bare silicon wafer. (b) Spin SU-8 negative photoresist on the wafer. (c) Expose and develop the resist. (d) Repeat for a total of four layers.

4.2.3 Fabricating the Mold

To begin the fabrication, a prebake was performed on the wafer by placing it on a hot plate for 5 minutes at 65ºC. The purpose of the prebake was to drive any residual moisture off the wafer and ensure a dry starting material. The wafer was placed in a spinner and excess SU-8, ~5 mL, was poured on the center of the wafer to ensure complete coverage. The wafer was spun to achieve an even coating of resist. The spinner was built by RHIT experts, and the spin step was 1 minute at 2000 rpm. The excess resist spun off the edge of the wafer and was contained in the spinner.

A soft bake was then performed for 5 minutes at 95ºC to begin to remove excess solvent and stabilize the resist. A Suss MicroTec MJB4 mask aligner was used to expose the wafer through the channel mask for 21 seconds of hard contact. The channel mask was designed in KLayout, a program for designing photolithography masks, and the design is shown in Figure 4.2.3.1.

The channel was 16 mm by 800 μm. The mask was made of plastic sheeting and was ordered from Output City in Bandon, OR. The mask was attached to a blank glass plate in order to interface with the aligner and is shown in Figure 4.2.3.2.

Figure 4.2.3.1: The mask design for the channel.

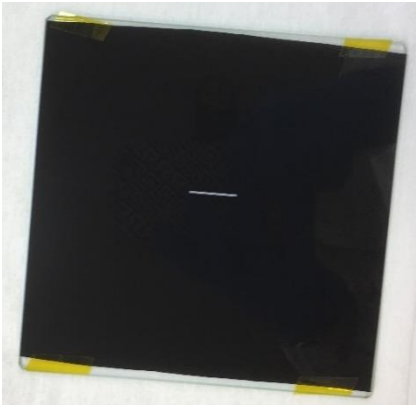

Figure 4.2.3.2: The channel mask attached to a glass plate to connect with the mask aligner.

A two-step post exposure bake was performed to stabilize the resist further. The first step was 1 minute at 65ºC and the second step was 1 minute at 95ºC. The resist was developed in SU-8 developer, which is primarily 1-methoxy-2-propyl acetate. The wafer was placed in a bath of the developer and agitated manually for 1 minute. The wafer was then moved to an isopropyl alcohol bath and agitated manually for 10 seconds. Finally, the wafer was placed in a bath of deionized (DI) water and agitated manually for 5 seconds. The developer, isopropyl alcohol, DI water process was repeated a second time to finish removing the unexposed resist. The wafer was then rinsed under a DI water stream and spun dry. A hard bake was performed at 160ºC for 5 minutes to drive off any residual moisture and finish the crosslinking of the resist, as shown in Figure 4.2.3.3.

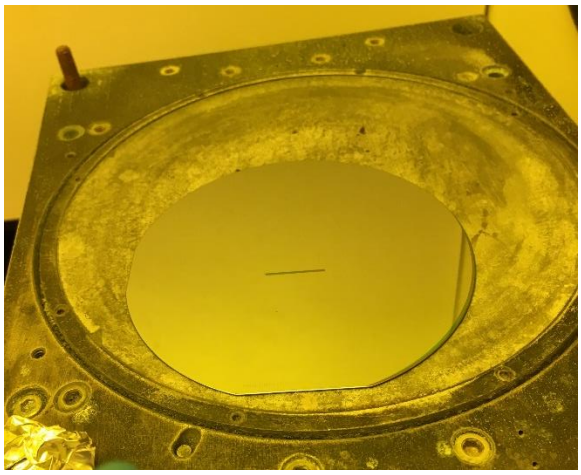

Figure 4.2.3.3: The wafer with the resist that forms the mold during the hard bake.

The patterning process, from the spin coat to the hard bake, was repeated a total of four times to thicken the resist. The prebake was not repeated, as the hard bake was sufficient to remove moisture between layers. The geometry of the channel was too small to measure the thickness of the resist with the Filmetrics Thin Film Measurement system, but this procedure was designed by MiNDS cleanroom facility experts and tested to show each layer is approximately 7 μm. Therefore, in total, the mold for the channel is ~28 μm tall, 800 μm wide, and 16 mm long.

4.2.4 PDMS Casting Process Flow

The process flow for casting the PDMS channel is shown below. The channel process flow is summarized in Figure 4.2.4.1.

1. Mix PDMS: 30 mL of the monomer base with 3 mL of the curing agent.
2. Use a vacuum chamber to remove bubbles introduced by mixing.
3. Pour PDMS over the mold.
4. Cure for 10 minutes at 150ºC.
5. Cut the channel out of the mold with a razor.
6. Cut access ports to the channel with a syringe.

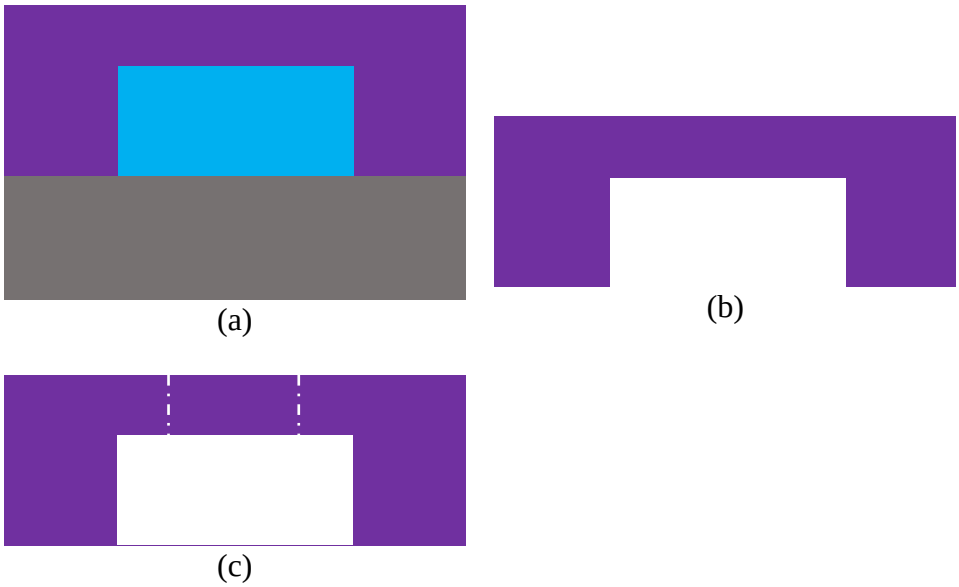

Figure 4.2.4.1: Illustrations of the process flow for casting the PDMS channel using the mold. Grey is the silicon, blue is SU-8 negative photoresist, and purple is the PDMS. (a) Pouring the PDMS over the mold. (b) Removing the channel from the mold with a razor after curing. (c) Cutting access ports to the channel with a syringe.

4.2.5 Casting the PDMS Channel

The elastomer used to make the channel was polydimethylsiloxane (PDMS). The elastomer was prepared by mixing 30 mL of the monomer base with 3 mL of the curing agent. Due to the

viscosity of the monomer, bubbles were introduced during the mixing step. The mixture was placed in an airtight chamber, and a vacuum was applied with an air pump to remove the bubbles, as shown in Figure 4.2.5.1. The vacuum step lasted ~90 minutes and ran until no bubbles were observed. Mixed PDMS takes ~2 hours to double in viscosity, so the vacuum step fell within the acceptable shelf life window. If the mixture becomes too viscous, pouring becomes more challenging. Pouring the PDMS before the viscosity doubles ensures a smooth pour.

Figure 4.2.5.1: The vacuum chamber that was used to remove bubbles from the PDMS. The tube was connected to an air pump.

The wafer with the mold for the channel was placed in a glass petri dish, and the PDMS was gently poured over the mold to avoid introducing new bubbles. The dish was placed in a 150ºC oven for 10 minutes to cure. After the dish cooled to room temperature, it was stored for 24 hours to ensure it was completely cured. A razor was then used to cut the channel out of the mold. The channel set at an angle to the mold is shown in Figure 4.2.5.2.

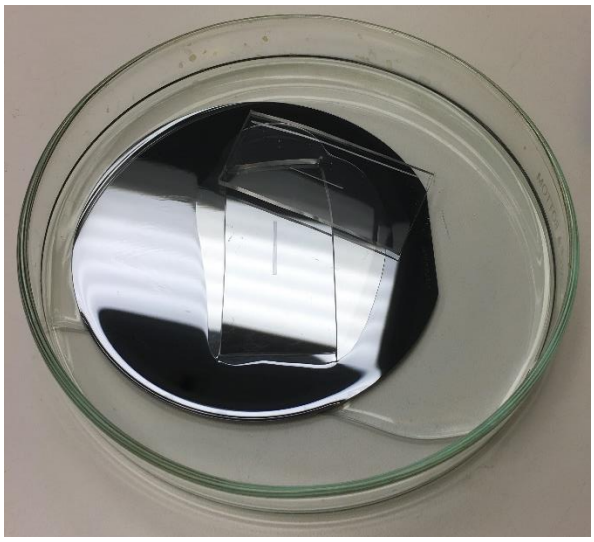

Figure 4.2.5.2: The PDMS channel in the mold.

After the form of the channel was cast in PDMS, it was necessary to add a way for fluids to be added and removed from the channel. A 21 gauge, 1 mL syringe was used to cut holes through the PDMS to the channel, as shown in Figure 4.2.5.3. The syringe was also used to place fluid in the channel during testing.

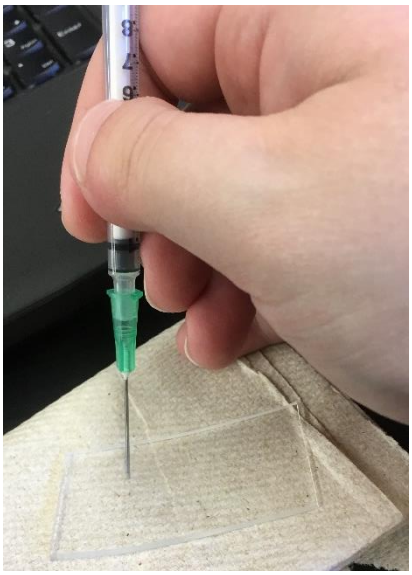

Figure 4.2.5.3: Using a syringe to cut holes in the PDMS to access the channel.

4.3 Fabrication of the Electrodes

4.3.1 Electrode Fabrication Overview

The electrodes consisted of titanium on a glass slide. To fabricate the electrodes, a thin film of titanium was deposited on the surface of a glass slide. Photoresist was used to protect the desired portions of the titanium as the excess was etched away. After the etch step, the remaining photoresist was removed.

4.3.2 Electrode Process Flow

The process flow for the electrodes is shown below. The electrode process flow is summarized in Figure 4.3.2.1.

1. Start with a clean, bare glass slide.
2. Deposit 200 nm of titanium with the electron beam physical vapor deposition (PVD) tool.
3. Spin SPR3622 positive photoresist on the slide.
4. Soft bake for 30 seconds at 90ºC.
5. Expose for 30 seconds of hard contact through the electrode mask.
6. Post-exposure bake for 30 seconds at 90ºC.
7. Develop.
8. Etch for ~10 seconds in 0.5% HF.
9. Use acetone and methanol rinses to remove the remaining photoresist.

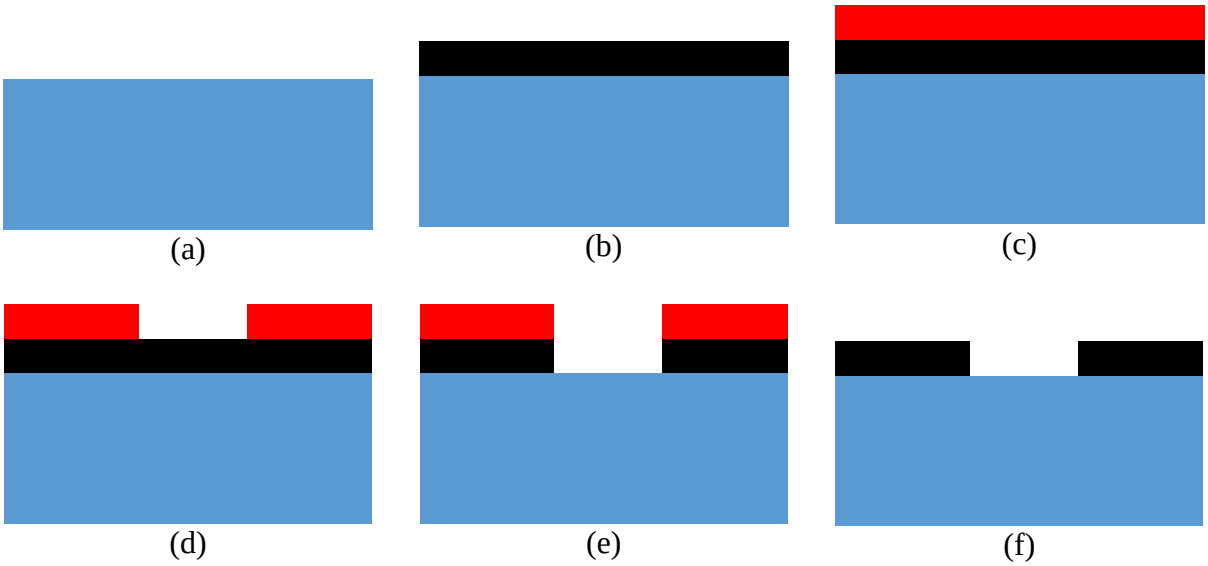

Figure 4.3.2.1: Illustrations of the process flow for fabricating the electrodes. Blue is the glass, black is titanium, and red is SPR3622 positive photoresist. (a) Clean, bare glass slide. (b) Use electron beam PVD to deposit 200 nm titanium. (c) Spin on SP3622 positive photoresist. (d) Expose and develop the resist. (e) Etch the titanium. (f) Remove remaining photoresist.

4.3.3 Electrode Deposition

To form the electrodes, a glass slide and a PVD75 Kurt J. Lesker electron beam physical vapor deposition system, shown in Figure 4.3.3.1, were used. Electron beam evaporation systems use a magnetically controlled stream of electrons to bombard a target material, knocking the target material out of a crucible and towards a substrate [33]. The pressure of the chamber is kept low to increase the path length of the target material and ensure it reaches the substrate and precipitates, forming a thin layer. A diagram of an electron beam evaporation system is shown in Figure 4.3.3.2.

Figure 4.3.3.1: The PVD75 Kurt J. Lesker electron beam physical vapor deposition system.

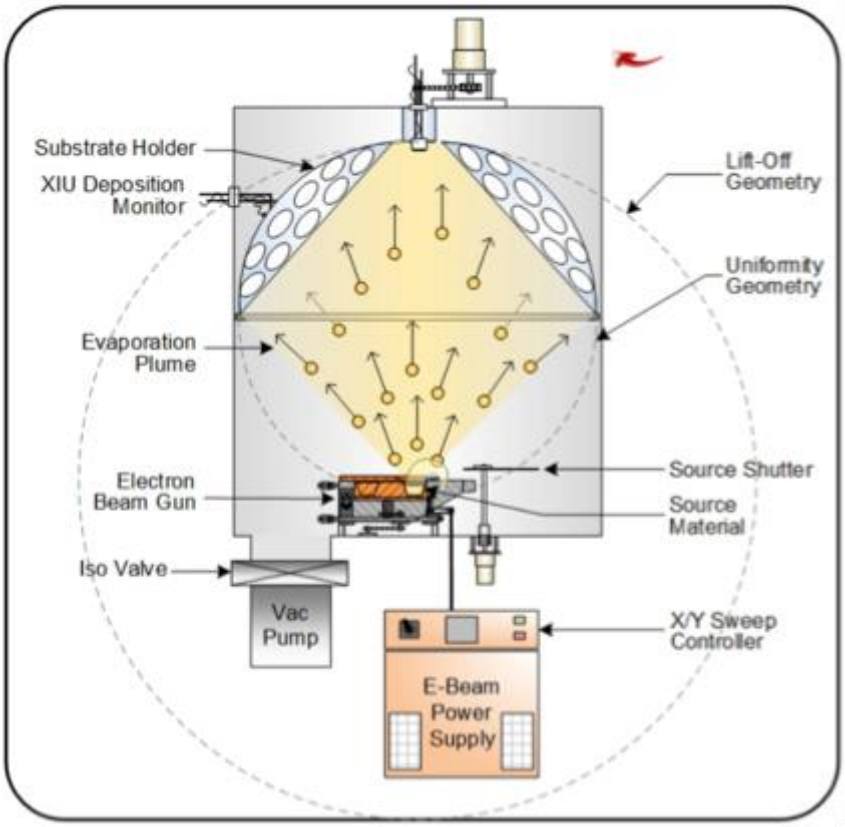

Figure 4.3.3.2: A diagram of an electron beam evaporation system [33].

The PVD75 electron beam evaporation system was used to deposit a 200. nm thick layer of titanium on the glass slides to form the electrodes, as shown in Figure 4.3.3.3. The layer was measured with the built-in in situ monitoring system.

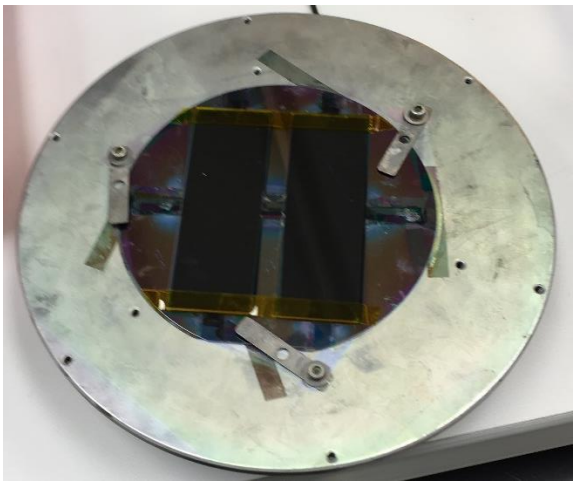

Figure 4.3.3.3: The deposited titanium layer on the glass slides in the holder for the electron beam system.

4.3.4 Electrode Patterning

The titanium was patterned in a process similar to the patterning of the mold. Since the titanium deposition step formed a thin layer on the whole glass slide, certain portions needed to be removed to form the desired shape for the electrodes. Photoresist was used to protect the desired portions of titanium while the extra portions were etched away. An adapter was attached to the spinner to hold the glass slide. SPR3622 positive photoresist was chosen for the patterning step, as it is the standard photoresist used in this cleanroom, and there were no extenuating circumstances. Excess resist was poured in the center of the glass slide, ~5 mL, and the glass slide was spun at 5500 rpm for 30 seconds to obtain an even coating of photoresist, as shown in Figure 4.3.4.1. A soft bake was performed at 90ºC for 30 seconds to begin removing excess solvent.

Figure 4.3.4.1: The spun glass slide in the adapter for the spinner.

Two designs of the electrodes were fabricated. Both electrode masks were designed in KLayout, and the designs are shown in Figure 4.3.4.2 and Figure 4.3.4.3. They were made of plastic sheeting and ordered from Output City in Bandon, Oregon.

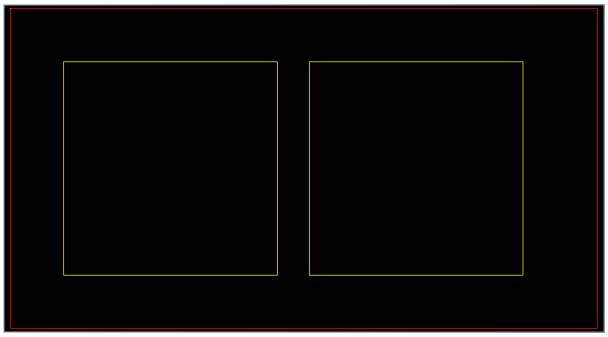

Figure 4.3.4.2: The first mask design for the electrodes.

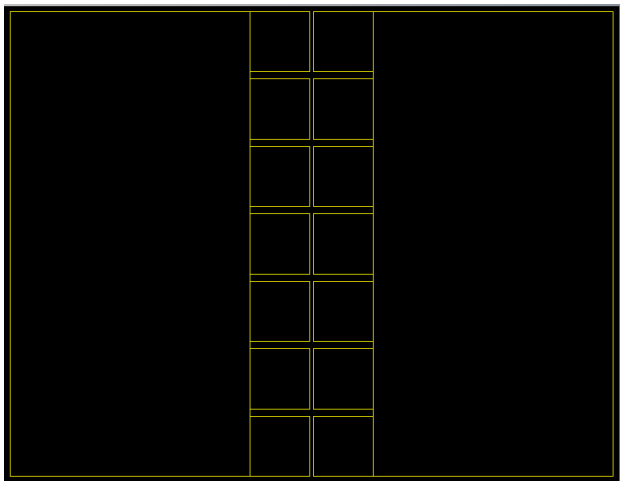

Figure 4.3.4.3: The second mask design for the electrodes.

The electrodes in Figure 4.3.4.2 were 4 mm square and 600 μm apart. The electrodes in Figure 4.3.4.3 had center squares that were 4mm by 4 mm; the electrodes were separated by 200 μm, and the squares were separated by 500 μm. The extensions behind the teeth were 16 mm to ensure they would cover the full width of the glass slides. The masks were attached to glass plates for structure and ease of handling. The masks on the glass slides are shown in Figure 4.3.4.4 and Figure 4.3.4.5.

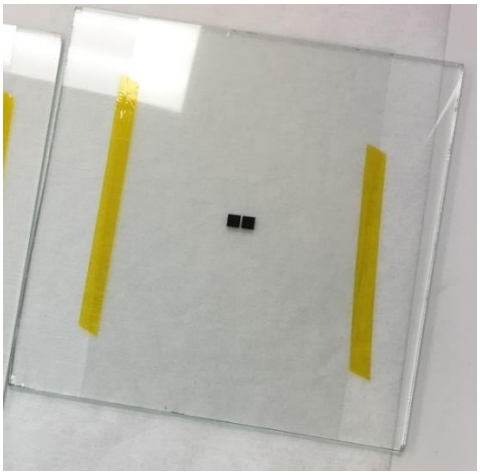

Figure 4.3.4.4: The first electrode mask attached to a glass plate.

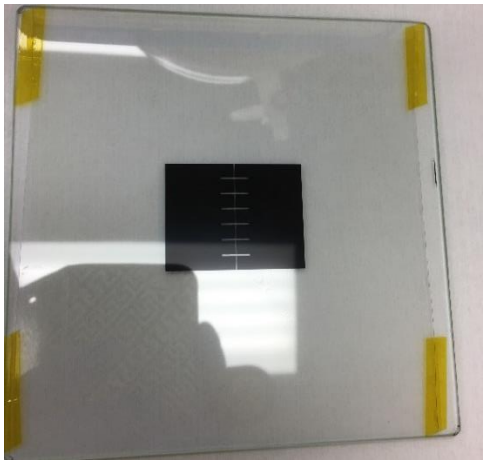

Figure 4.3.4.5: The second electrode mask attached to a glass plate.

For each design, the electrode mask was placed in hard contact with the glass slide, as shown in Figure 4.3.4.6. An additional glass plate underneath the slide was used for ease of handling. The stack was placed in an ELC-500 Light Exposure System by Electro-Lite

Corporation, as shown in Figure 4.3.4.7. The ELC-500 was used to expose the stack to UV light for 30 seconds.

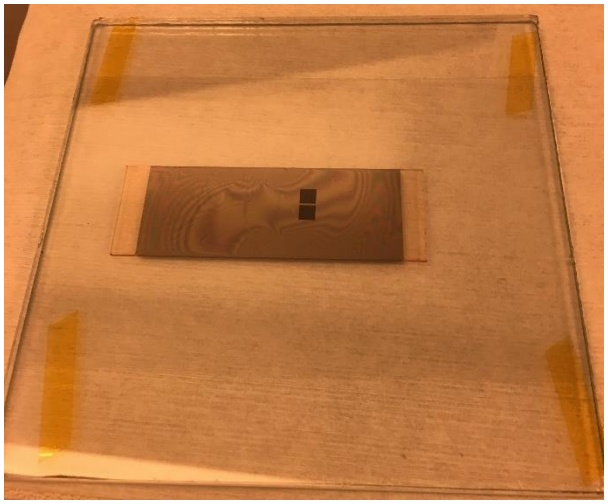

Figure 4.3.4.6: The glass slide in hard contact with the electrode mask. An additional glass plate was placed under the glass slide for ease of handling.

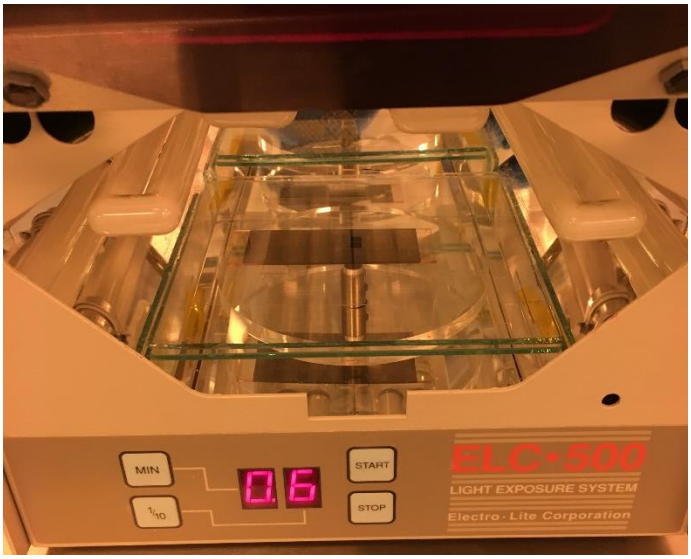

Figure 4.3.4.7: The ELC-500 Light Exposure System by Electro-Lite Corporation with the electrode mask and glass slide stack.

A post exposure bake was performed at 90ºC for 30 seconds to stabilize the resist. The slide was placed in a bath of SPR3622 developer and agitated. The slide was removed from the bath when the undesired portions of resist had washed away as determined visually, ~30 seconds. The slide was rinsed under a stream of DI water and blown dry with nitrogen. The titanium was

etched in a solution of 0.5% HF for ~10 seconds until the undesired regions of titanium had etched away, as determined visually. Two DI rinses were performed following the HF etch, and the slide was blown dry with nitrogen. Acetone and methanol rinses were used to remove the remaining photoresist from the slide. A final DI rinse of the slide was performed, and the slide was blown dry with nitrogen. The final slides with the electrodes are shown in Figure 4.3.4.8 and Figure 4.3.4.9. The extra portions of titanium remaining on the edges of the slide are an artifact of the way the spinner adapter interacts with the glass slide and the photoresist, and they do not impact the performance of the device.

Figure 4.3.4.8: The completed electrodes of the first design.

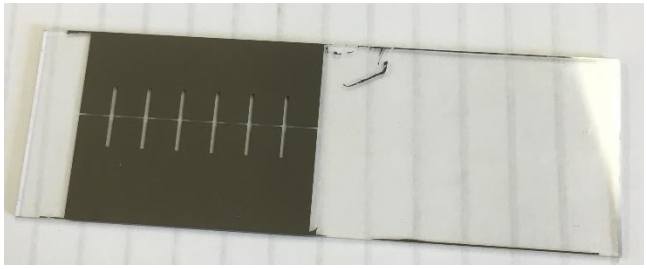

Figure 4.3.4.9: The completed electrodes of the second design.

4.4 Assembly

To run the device, the separately fabricated pieces were combined. See Figure 4.1 for the cross section. The goal was to align the channel over the electrodes as shown in Figure 4.4.1 so that the channel contacted both electrodes. The contact on both electrodes was required to allow

current to flow through the working fluid. If one of the electrodes did not touch the fluid, the circuit would be open and no current would flow.

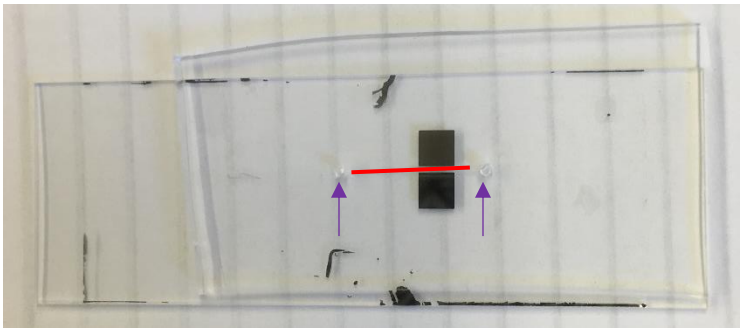

Figure 4.4.1: The channel and electrodes aligned. The red line has been added to indicate the location of the channel, as it is not visible in the image. The purple arrows indicate the holes at the ends of the channel.

Following the hand alignment, it was necessary to connect the electrical components. An Arduino Uno was used to control the MHD micropump. Wires were used to connect the electrodes to the Arduino by sandwiching them between the PDMS and the glass slide, as shown in Figure 4.4.2. The connected Arduino is shown in Figure 4.4.3.

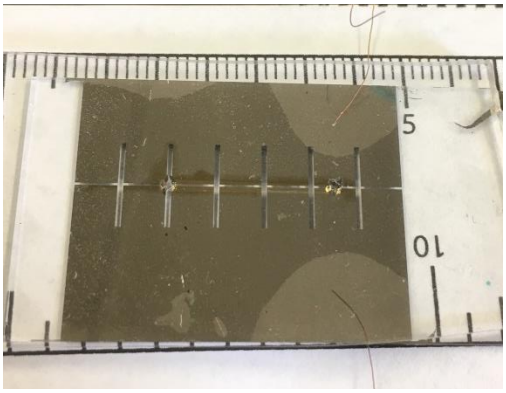

Figure 4.4.2: Wires connecting the electrodes to the Arduino.

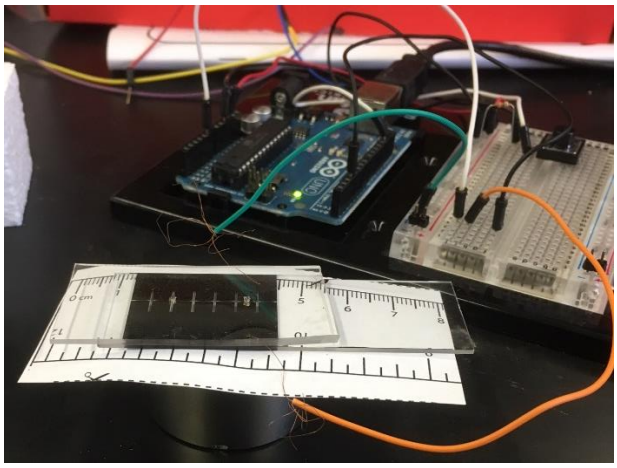

Figure 4.4.3: The Arduino connected to the MHD micropump.

In addition to connecting the electrodes and applying a 5 V potential, the Arduino was used to test whether a current was truly flowing through the electrolytic solution. An additional wire was connected to the Arduino as an input and a numerical output was printed in a serial monitor on the computer. When current was flowing through the fluid, the numerical output was nonzero. This provided an extra check to ensure the electrical current component was functioning correctly. With the electrical components successfully connected, the channel was placed atop a permanent magnet to complete the MHD micropump. The permanent magnet was measured to have a magnetic field strength of 8.242 mT $\pm$ 0.004 mT with a Vernier Magnetic Field Sensor. To control the pump, a pushbutton was integrated with the Arduino. When pushed, the electrical component was turned on. The code controlling the device is available in Appendix A.

4.5 Testing

For each trial, two solutions were used. The two solutions used in each trial had the same concentration of NaCl, but one was dyed with erioglaucine disodium salt for visibility. The goal was to measure fluid velocity through the channel. The blue dye allowed visible tracking of the location of the boundary between the dyed and colorless solutions. Salt concentrations were 0.01

M, 0.1 M, 0.5 M, and 1 M. The erioglaucine concentration was different for each data set, but was as close to 2.5 mM as measurement constraints allowed. The colorless NaCl solution was placed in the channel and droplets of the dyed solution were placed at the inlet and outlet, as shown in Figure 4.5.1. A camera was positioned above the pump and was used to record the trial and track the progress of the dyed solution through the channel. The applied voltage was 5 V.

It should be noted that other methods of tracking the fluid motion were considered. Tartrazine dye at 0.5 g/L was considered for the dyed solution. However, the yellow color of the dye was challenging to observe in the thin channel. Another potential method for tracking fluid flow through the channel is to add microbeads to the working fluid and view the channel through a microscope. However, the channel was smaller than the microbeads available in the lab and purchasing smaller beads was cost prohibitive, as size control requires expensive processing. Additionally, there were concerns about placing the strong magnet on the microscope stage.

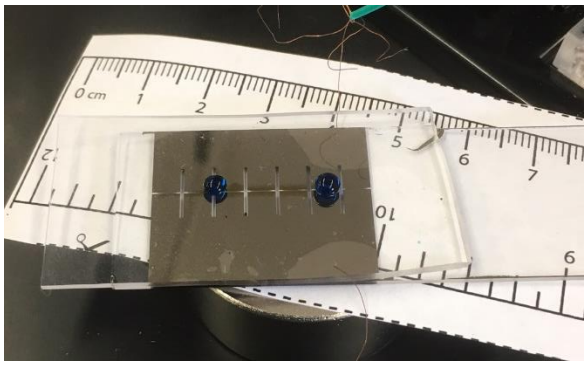

Figure 4.5.1: The colorless solution in the channel with the dyed solution at the inlet and outlet ports.

Between trials, the PDMS channel was lifted away from the glass slide and both were thoroughly cleaned. Both were air dried before beginning the next trial.

5. RESULTS AND DISCUSSION

5.1 Initial Device Testing

Early tests revealed that the first design of the electrodes, the simple square design, resulted in no fluid motion. This electrode design only contacted fluid in a quarter of the length of the channel. Current through the fluid was registered, but it did not provide enough force to cause fluid motion. Additionally, the electrodes were spaced such that alignment of the channel ensuring the fluid would contact both electrodes was challenging. The second design of the electrodes, however, was successful. This design spanned the full length of the channel and provided enough force to cause fluid flow. The electrodes were also 400 μm closer together, simplifying the alignment. The success of the second design was attributed to the additional force lent by spanning the full length of the channel. The first design did not have sufficient driving force to overcome the viscous forces present within the working fluid. Extending the electrodes was sufficient to overcome the viscous forces and drive fluid flow.

5.2 Impact of PWM

Solutions for the first set of trials with the working electrode design were prepared individually. The apparent velocity of fluid through the channel was calculated from the measured distance traveled and time required as read from the captured videos. The velocity calculation was

$$v = \frac{\left(60\frac{s}{min}\right) \cdot d}{t} \tag{5.1.1}$$

where v is the velocity in millimeters per minute, d is the distance in millimeters, and t is the time in seconds. The calculated apparent velocity assumes a uniform velocity profile, and does not account for surface effects. However, the apparent velocity is a way to quantitatively compare

different experimental conditions. The results are shown in Figure 5.1.1. To verify that the fluid flow was indeed in the Stokes regime, the Reynolds number was calculated. The Reynolds number was calculated using

$$Re = \frac{\rho v L}{\mu} \qquad 5.1.2$$

The Reynolds number for the highest velocity, 3.5 mm/min, was 0.0035 < 0.1, confirming Stokes flow for all trials.

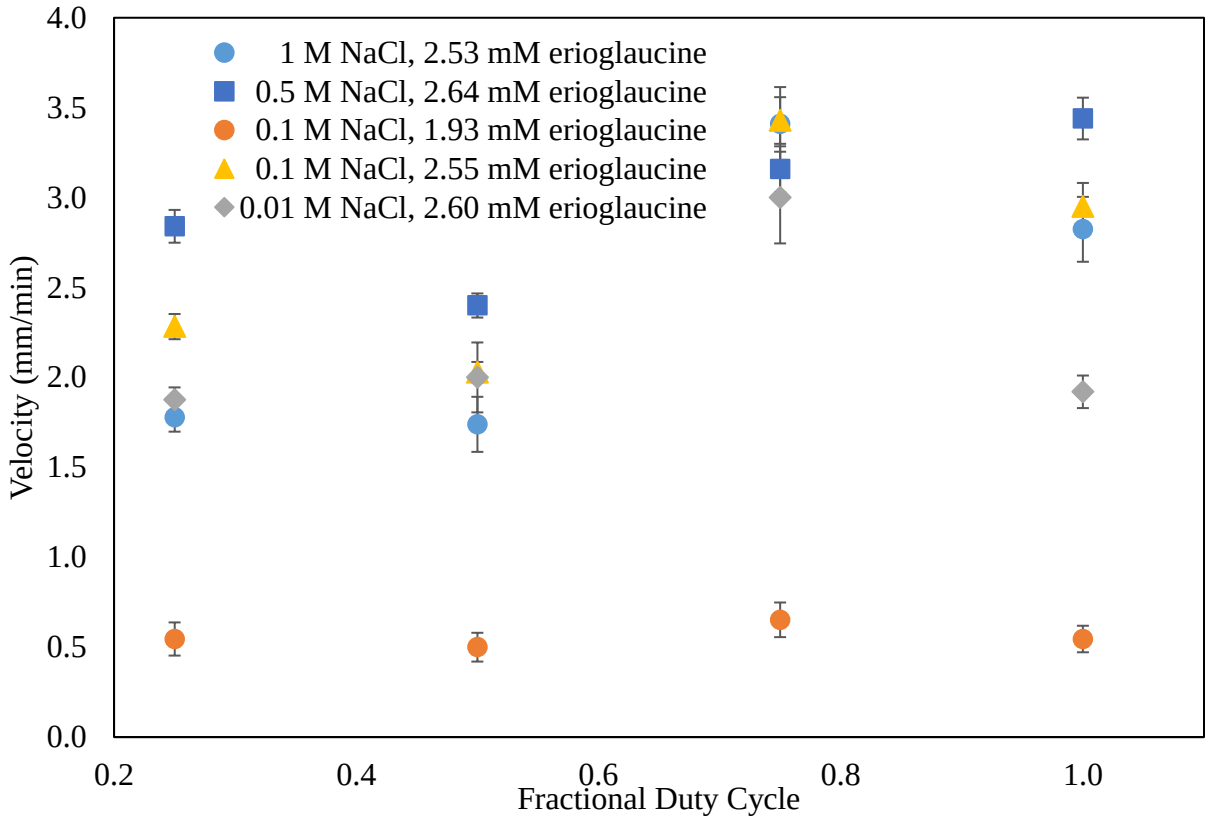

Figure 5.2.1: Apparent fluid velocity through the MHD micropump as a function of the duty cycle, with variable NaCl and erioglaucine disodium salt concentrations. Each data point represents a single trial.

The error in the distance traveled was 0.1 mm and the error in the time was between 5 and 15 seconds based on the read error of the individual video. Error propagation was performed to calculate the error bars shown in Figure 5.1.1 from the error in the measured values of the time

and the distance traveled. The error propagation calculation can be found in Appendix B. The greatest contribution to error was uncertainty in the time measurement.

There are several trends in the data. First, the duty cycle was expected to mitigate the effects of electrolysis. This was expected to manifest as a reduction in bubble formation. However, no bubbles were observed in this device. Instead, the electrolysis reduction manifested in an increase in flow rate. For four out of the five data sets, the flow rate is highest at 75% duty cycle. The largest increase in the flow rate is seen in the 0.01 M NaCl data set, where the 75% duty cycle velocity is 1.5 times the 100% duty cycle velocity. The velocities of the 25% and 50% duty cycle conditions were within experimental error for four of the data sets.

The increase in velocity from 100% duty cycle to 75% duty cycle is due to the reduction in side reactions that occur at the electrodes. Electrolysis is the breakdown of water into hydrogen and oxygen gas, and occurs at the electrodes when an electrical current is running through the working fluid. The short interval of no electrical current with a reduced duty cycle temporarily stops the side reactions, such as electrolysis. When the electrical current is constantly flowing, the reactions are constantly occurring and can create a boundary layer of hydrogen and oxygen at the electrodes. The boundary layer limits the portion of the channel that can be used to transport fluid. However, there is a limit to the benefit of the reduced duty cycle, as evidenced by the lower velocities at 50% and 25% duty cycle. At the lower values, the longer time without driving force reduced the apparent velocity.

5.3 Impact of Salt Concentration

Another interesting result is the effect of salt concentration on the apparent velocity. The expected result was decreasing the salt concentration would decrease the apparent flow rate. The

intention was to keep the concentration of the erioglaucine disodium salt, the blue dye, consistent between data sets. However, measuring masses on the order of 0.002 g is challenging to keep perfectly similar. The result was slight variations in the erioglaucine disodium salt concentration. The apparent velocity results in Figure 5.2.1 show a stronger dependence on the erioglaucine disodium salt concentration than on the salt concentration. The dataset with the lowest concentration of erioglaucine disodium salt also has the lowest apparent velocity, though it does not have the lowest salt concentration.

To isolate the effects of salt concentration on the apparent velocity, a stock solution of erioglaucine disodium salt was prepared. The same erioglaucine disodium salt stock solution was used to make each of the dyed salt solutions, keeping the erioglaucine disodium salt concentration consistent across data sets. The results are shown in Figure 5.3.1.

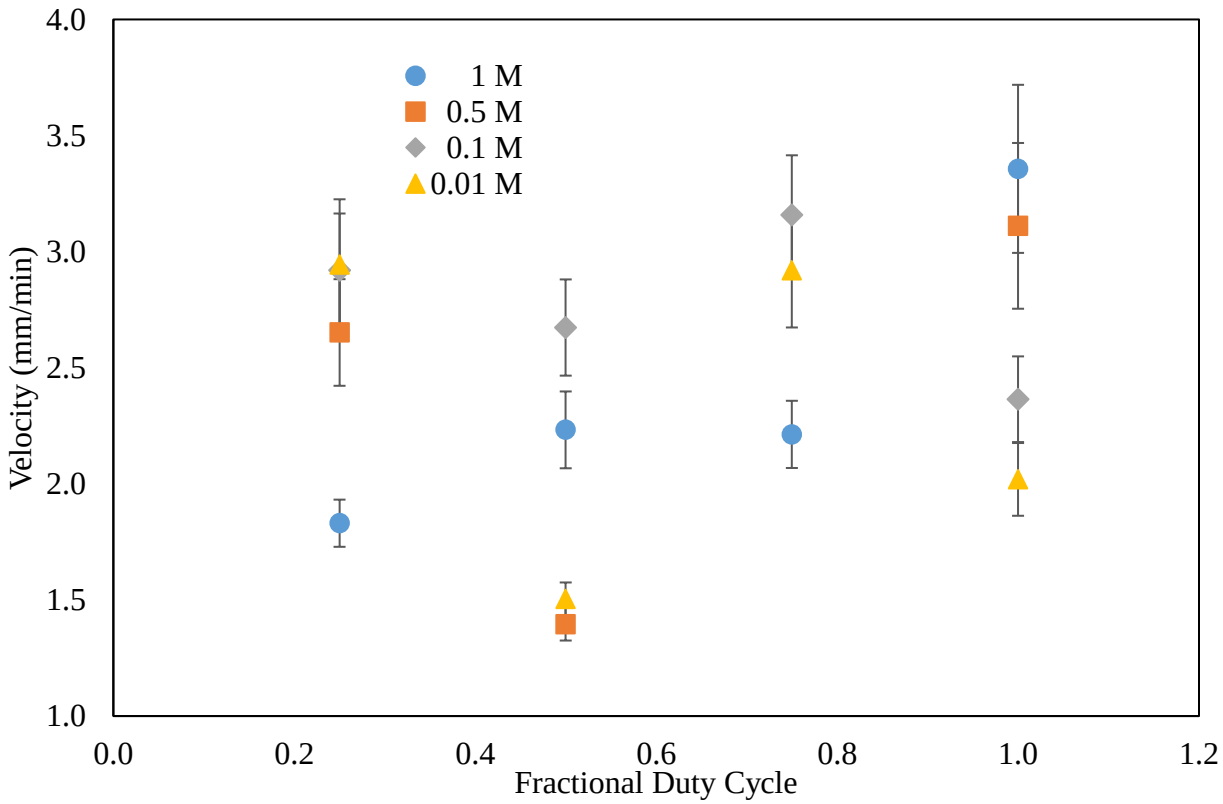

Figure 5.3.1: Apparent fluid velocity through the MHD micropump as a function of the duty cycle, with variable NaCl, holding the erioglaucine disodium salt concentration constant at 2.5 mM.

At 100% duty cycle, the apparent fluid velocity decreases with decreasing NaCl concentration. However, the other duty cycle levels do not follow the same pattern. In fact, at 25% duty cycle, three of the points are within experimental error. Removing the variability in the erioglaucine disodium salt concentration did not illuminate a strong dependence on the salt concentration. The effect of the NaCl concentration on the velocity through the channel is unclear given these data. The erioglaucine disodium salt concentration appears to have a larger impact on the apparent velocity than the salt concentration.

The structure of the erioglaucine disodium salt, shown in Figure 5.3.2, is likely responsible for the velocity dependence. The Lorentz force acts upon charged species, and the remainder of the fluid motion is due to momentum diffusion. NaCl only dissociates to two charged species, Na^+ and Cl^-, whereas erioglaucine disodium salt dissociates to form three charged species, $2Na^+$ and EG^{2-}. The largest ion also has four charges. The larger number of charged species and charges increases the impact of the Lorentz driving force on the fluid. Regardless of whether the charge is negative or positive, the Lorentz force is in the same direction. The larger size of the dye molecule also increases the surface area for collisions with the surrounding fluid, improving momentum transfer. The similarity in the flowrates in Figure 5.3.1 is likely accounted for by the consistent concentration of erioglaucine disodium salt, even in the presence of a varying salt concentration.

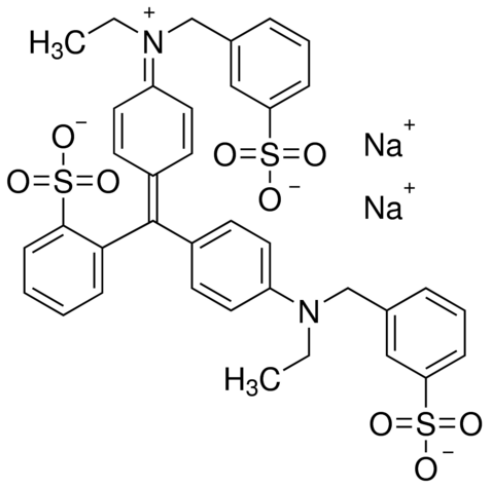

Figure 5.3.2: The chemical structure of erioglaucine disodium salt [34].

5.4 Titanium Performance

Throughout testing, a yellow discoloration was observed on the electrodes where they came into contact with the fluid. The discoloration is shown in Figure 5.4.1, and appeared to have no impact on the experimental results. Since early tests were performed with the yellow tartrazine dye, the discoloration was considered to be a result of the dye. However, placing a drop of the tartrazine solution on the outer corner of the electrode resulted in no discoloration. The yellow discoloration continued to occur when using the blue erioglaucine disodium salt dye.

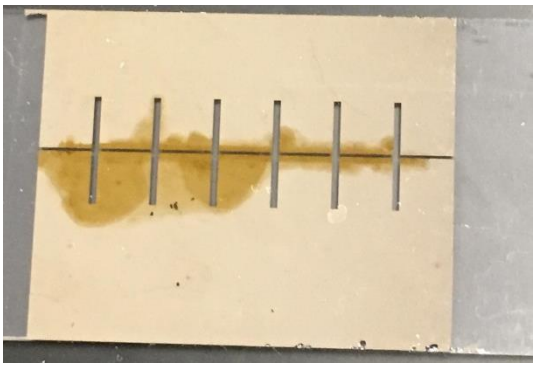

Figure 5.4.1: The yellow discoloration observed on the titanium electrodes.

The discoloration is a result of titanium anodization, which is "an electrolytic oxidation process for thickening the oxide layer on active titanium metals" [35]. The color of the resulting

thin oxide film is due to wave interference in the crystal lattice [35]. Some of the light is reflected off the surface of the oxide, and some is refracted through the oxide and reflects off the surface of the metal. The difference in path length creates a phase shift, and results in constructive or destructive interference for different wavelengths [36]. The interference is observed as a color change. The anodizing voltage controls the thickness of the grown oxide, and the thickness of the oxide determines the observed color. A 5 V potential results in a yellow color [35], as shown in Figure 5.4.1.

5.5 Other Results

Following completion of data collection for the constant erioglaucine disodium salt conditions, a crack in the PDMS radiating from the inlet port was discovered. The crack did not go through the entire thickness of the PDMS, but rather was on the surface near the channel. It was only discovered when peeling the PDMS away from the glass for cleaning, and was not visible when the PDMS was flat. Though the crack was small, it allowed liquid to leak between the PDMS and the glass slide. When the pump was run after the crack formed, no motion was observed. The crack indicated the PDMS fabrication method is best suited to disposable or temporary applications, rather than repeated use.

A standard operating procedure (SOP) was written for running the micropump, and is available in Appendix C.

6. CONCLUSIONS AND RECOMMENDATIONS

An effective MHD micropump was fabricated with a PDMS channel and titanium electrodes supported on a glass slide with a permanent magnet. An electrode design that spanned

the full length of the channel was successful in driving fluid motion, whereas an electrode design spanning a quarter of the length of the channel was not successful in driving fluid motion.

The pump was driven using an Arduino microcontroller to control the electrical potential. Erioglaucine disodium salt blue dye was used to track fluid motion through the channel. It appeared that the concentration of erioglaucine disodium salt had a greater impact on the apparent fluid velocity than the NaCl concentration, likely as a result of the greater number of ions, greater number of charges, and larger molecule size. The impact of NaCl concentration on the velocity through the channel was unclear. A 75% duty cycle was found to result in the greatest fluid velocity, meaning a 75% duty cycle offers improved performance for DC MHD micropumps.

The combination of the electrolytic solution and the electrical potential anodized the titanium that contacted the working fluid, making titanium electrodes best suited for disposable applications. The anodization could serve as an effective visual determination of whether the device is truly delivering an electrical potential to the fluid in a portable application. The crack in the PDMS also indicates it is best for permanently bonded or disposable applications. Many lab-on-a-chip devices are designed for medical applications, and are disposable devices. These fabrication techniques would be ideal for such medical applications.

Overall, previous research and this study have shown proof of concept of MHD micropumps. Future study should first focus on quantitatively fully characterizing the MHD micropump. Then, research should shift to creating more complex systems that incorporate multiple species to model multiple reactants. Then, MHD micropumps can be applied to specific lab-on-a-chip devices.

Future studies should begin by exploring another method for tracking fluid flow that does not introduce additional ions to the working fluid. This is the biggest hurdle to fully understanding

the operation of the micropump, and could include other dyes or small beads. A tracking method that does not introduce additional ions is critical for isolating the NaCl concentration and quantifying its impact on the apparent fluid velocity. A neutral dye would use the same experimental setup without confounding the results. Another area of future study is isolating the erioglaucine disodium salt concentration to quantify its impact on the velocity through the channel. Quantifying the impact of each species individually may elucidate the trends seen in this study.

Once the tracking method is refined, the next step will be optimizing the device. Alternative electrode geometries should be studied to see whether they improve fluid flow through the channel. Another area for future study is alternative channel geometries to better model lab-on-a-chip devices, and investigate fabricating multiple MHD micropumps on a single chip to control mixing of multiple species. Many lab-on-a-chip devices require multiple reactants and samples, and designing a device to incorporate multiple solutions would best model the final application. With a more complex geometry, studying the time required to deliver a reactant to the reactor location will be critical.

LIST OF REFERENCES

[1] "Microfluidics and Microfluidic Devices: A Review." *Elveflow*, 2018, http://www.elveflow.com/microfluidic-tutorials/microfluidic-reviews-and-tutorials/microfluidics-and-microfluidic-device-a-review/. Accessed 28 May 2018.

[2] Kitson, Philip; Rosnes, Mali; Sans, Victor; Dragone, Vincenza; and Cronin, Leroy. "Configurable 3D-Printed millifluidic and microfluidic 'lab on a chip' reactionware devices." *Lab Chip*, vol. 12, 2012, pp. 3267-3271, DOI: 10.1039/c2lc40761b. Accessed 28 May 2018.

[3] Li, Dongqing. *Electrokinetics in Microfluidics.* Elsevier, 2004.

[4] Singhal, Vishal; Garimella, Suresh; and Raman, Arvind, "Microscale pumping technologies for microchannel cooling systems." *Birck and NCN Publications*, Paper 84, 2004, http://docs.lib.purdue.edu/nanopub/84. Accessed 28 May 2018.

[5] Abhari, Farideh; Jaafar, Haslina; and Ynus, Nurul, "A Comprehensive Study of Micropumps Technologies." *Int. J. Electrochem. Sci.*, vol. 7, 2012, pp. 9765-9780, http://www.electrochemsci.org/papers/vol7/71009765.pdf. Accessed 28 May 2018.

[6] Iverson, Brian D. and Garimella, S V., "Recent Advances in Microscale Pumping Technologies: A Review and Evaluation." *CTRC Research Publications*, Paper 89, 2008, http://dx.doi.org/10.1007/s10404-008-0266-8. Accessed 28 May 2018.

[7] Nguyen, Nam-Trung, "Micro magnetofluidics – interactions between magnetism and fluid flow on the microscale." *Microfluidics and Nanofluidics*, vol. 12, 2012, pp. 1-16, https://dr.ntu.edu.sg/bitstream/handle/10220/7689/HighlightedRevision.pdf?sequence=1. Accessed 30 May 2018.

[8] George, Thompson, "Electromagnetic pump for electrically conducting liquids." US2386369A, United States Patent and Trademark Office, 4 June 1943.

[9] Godbold, Nat, "Electromagnetic fluid pump." US2655107A, United States Patent and Trademark Office, 1 September 1950.

[10] Carlson, William, and Exner, Frank, "Electromagnetic Conductive Fluid Pump." US3045599A, United States Patent and Trademark Office, 8 June 1959.

[11] Lindenblad, Nils, "Electromagnetic Induction Pump." US2807212A, United States Patent and Trademark Office, 12 December 1952.

[12] Hughes, M.; Pericleous, K. A.; and Cross, M., "The numerical modelling of DC electromagnetic pump and brake flow." *Applied Mathematical Modeling*, vol. 19, no. 12, 1995, pp. 713-723, https://doi.org/10.1016/0307-904X(95)00110-6. Accessed 1 June 2018.

[13] Jang, Jaesung, and Lee, Seung, "Theoretical and experimental study of MHD (magnetohydrodynamic) micropump." *Sensors and Actuators A: Physical*, vol. 80, no. 1, 2000, pp. 84-89, https://doi.org/10.1016/S0924-4247(99)00302-7. Accessed 1 June 2018.

[14] Lemoff, Asuncion, and Lee, Abraham, "An AC Magnetohydrodynamic Microfluidic Switch for Micro Total Analysis Systems." *Biomedical Microdevices*, vol. 5, no. 1, 2003, pp. 55-60, https://doi.org/10.1023/A:1024415400633. Accessed 1 June 2018.

[15] Patel, Vaibhav and Kassegne, Samuel Kinde, "Electroosmosis and thermal effects in magnetohydrodynamic (MHD) micropumps using 3D MHD equations." *Sensors and Actuators B: Chemical*, vol. 122, no. 1, 2007, pp. 42-52, https://doi.org/10.1016/j.snb.2006.05.015. Accessed 1 June 2018.

[16] Rivero, M., Cuevas, S., "Analysis of the slip condition in magnetohydrodynamic (MHD) micropumps." *Sensors and Actuators B: Chemical*, vol. 166-167, 2012, pp. 884-892, https://doi.org/10.1016/j.snb.2012.02.050. Accessed 1 June 2018.

[17] Lemoff, Asuncion and Lee, Abraham, "An AC magnetohydrodynamic micropump." *Sensors and Actuators B: Chemical*, vol. 63, no. 3, 2000, pp. 178-185, DOI: 10.1016/S0925-4005(00)00355-5. Accessed 1 June 2018.

[18] Lim, Sangsoo and Choi, Bumkyoo, "A study on the MHD (magnetohydrodynamic) micropump with side-walled electrodes." *Journal of Mechanical Science and Technology*, vol. 23, 2009, pp. 739-749, DOI 10.1007/s12206-008-1107-0. Accessed 1 June 2018.

[19] Bao, Jian-Bin and Harrison, D. Jed, "Design and Fabrication of Microchannels for Magnetohydrodynamic Flow." *International Conference on MEMS, NANO and Smart Systems*, 23 July 2003, Banff, Alberta, Canada.

[20] Irshad, Wasim and Peroulis, Dimitrios, "A Silicon-Based Galinstan Magnetohydrodynamic Pump." *Power MEMS*, vol. 5, no. 1, 2009, pp. 127-129, https://www.researchgate.net/publication/267549805_A_SILICON-BASED_GALINSTAN_MAGNETOHYDRODYNAMIC_PUMP. Accessed 4 June 2018.

[21] Nguyen, Bao and Kassegne, Samuel, "High-current density DC magnetohydrodynamics micropump with bubble isolation and release system." *Microfluidics and Nanofluidics*, vol. 5, no. 3, 2008, pp. 383-393, DOI 10.1007/s10404-007-0255-3. Accessed 4 June 2018.

[22] Zhong, Jihua; Yi, Mingqiang; and Bau, Haim, "Magnetohydrodynamic (MHD) pump fabricated with ceramic tapes." *Sensors and Actuators A: Physical*, vol. 96, no. 1, 2002, pp. 59-66. https://doi.org/10.1016/S0924-4247(01)00764-6. Accessed 4 June 2018.

[23] Homsy, Alexandra; Koster, Sander; Eijkel, Jan; van den Berg, Albert; Lucklum, F.; Verpoortec, E.; and de Rooij, Nico, " A high current density DC magnetohydrodynamic (MHD) micropump." *Lab on a Chip*, vol. 5, 2005, pp. 466-471, DOI: 10.1039/b417892k. Accessed 4 June 2018.

[24] Kim, Chun; Lee, Jongkwang; and Kwon, Sejin, "Design, fabrication, and testing of a DC MHD micropump fabricated on photosensitive glass." *Chemical Engineering Science*, vol. 117, 2014, pp. 210-216. https://doi.org/10.1016/j.ces.2014.06.035. Accessed 4 June 2018.

[25] Bau, Haim; Zhong, Jihua; and Yi, Mingqiang, " A minute magneto hydro dynamic (MHD) mixer." *Sensors and Actuators B: Chemical*, vol. 79, 2001, pp. 207-215, https://doi.org/10.1016/S0925-4005(01)00851-6. Accessed 4 June 2018.

[26] Kang, Ho-Jin and Choi, Bumkyoo, "Development of the MHD micropump with mixing function." *Sensors and Actuators A: Physical*, vol. 165, no. 2, pp. 439-445, https://doi.org/10.1016/j.sna.2010.11.011. Accessed 4 June 2018.

[27] "PDMS: A Review." *Elveflow*, 2018, https://www.elveflow.com/microfluidic-tutorials/microfluidic-reviews-and-tutorials/the-poly-di-methyl-siloxane-pdms-and-microfluidics/. Accessed 4 June 2018.

[28] Hirzel, Timothy. "PWM." *Arduino*, 2018, https://www.arduino.cc/en/Tutorial/PWM. Accessed 25 June 2018.

[29] Henthorn, Dave. "Important CHE 502 Equations." *Rose-Hulman Institute of Technology*, 2018.

[30] Rhodes, Martin. "Introduction to Particle Technology." *John Wiley and Sons, Ltd*, 2008.

[31] Bird, Byron; Stewart, Warren; and Lightfoot, Edwin. "Transport Phenomena." *John Wiley and Sons, Inc*, 2006.

[32] "Positive vs. Negative Tone Photoresists." *Microchem*, 2018. http://www.microchem.com/Prod-LithographyOverviewPosNeg.htm. Accessed 12 August 2018.

[33] Hughes, Matt. "What is E-Beam Evaporation?" *Semicore*, 2016. http://www.semicore.com/news/89-what-is-e-beam-evaporation. Accessed 18 July 2018.

[34] "Erioglaucine disodium salt." *Sigma Aldrich*, 2018, https://www.sigmaaldrich.com/catalog/product/sial/861146?lang=en&region=US. Accessed 11 July 2018.

[35] Karambakhsh, Ali; Afshar, Abdollah; Ghahramani, Shahram; and Malekinejad, Pejman. "Pure Commercial Titanium Color Anodizing and Corrosion Resistance." *Journal of Materials Engineering and Performance*, 2011, vol. 20, no. 9, pp. 1690-1696, DOI: 10.1007/s11665-011-9860-0. Accessed 11 July 2018.

[36] Diamanti, Maria; Del Curto, Barbara; and Pedeferri, MariaPia. "Interference Colors of Thin Oxide Layers on Titanium." *Color Research and Application*, 2008, vol. 33, no. 3, pp. 221-228, https://doi.org/10.1002/col.20403. Accessed 11 July 2018.

APPENDICES

APPENDIX A: MHD MICROPUMP CODE

```
//MHD Micropump

//This code is designed to run an MHD micropump, controlling
//an electric field.
//Rose-Hulman Institute of Technology
//Designed by Rachel Weber
//Advisor: Dr. Anastasio

//Define the pin for the electric field
int elecPin = 3;

//Define the pin for a pushbutton input
int buttonPin = 13;

//Define a variable for reading the pushbutton status and
//initialize status as released
int value = HIGH;

//Define a pin for checking if a current is running through
//the fluid
int checkPin = 0;

//Define a variable for the numeric value of the potential at
//the checkPin location, initialize low
int check = 0;

void setup() {

  //Set the electric field pin to output
  pinMode(elecPin,OUTPUT);

  //Set the pushbutton pin to an input
  pinMode(buttonPin,INPUT);

  //Start the serial port at 9600 bps
  Serial.begin(9600);

}

void loop() {
  //Read the pushbutton
  value = digitalRead(buttonPin);

  //If the button is released, turn the pump off
  if(value == HIGH) {
```

```
  analogWrite(elecPin, 0);
 }
 //If the button is pushed, turn the pump on. This number can be
 //changed to adjust the duty cycle. 255, 100%. 191, 75%.
 //127, 50%. 64, 25%.
 else {
  analogWrite(elecPin, 64);
 }

 //Check if there is current running through the fluid
 check = analogRead(checkPin);

 //Print the numeric value
 Serial.println(check);
}
```

APPENDIX B: ERROR PROPAGATION

Since the velocity was calculated from two measured values, error propagation was required. The velocity calculation was

$$v = \frac{\left(60\frac{s}{min}\right)\cdot d}{t} \tag{B.1}$$

The error calculation was

$$error = \sqrt{\left(\frac{\partial v}{\partial d}\right)^2 d_{err}^2 + \left(\frac{\partial v}{\partial t}\right)^2 t_{err}^2} \tag{B.2}$$

where d_{err} is the error in the distance and t_{err} is the error in the time. The partial derivatives are

$$\frac{\partial v}{\partial d} = \frac{60\frac{s}{min}}{t} \tag{B.3}$$

$$\frac{\partial v}{\partial t} = -\frac{\left(60\frac{s}{min}\right)\cdot d}{t^2} \tag{B.4}$$

Combining Equations B.3 and B.4 with Equation B.2, the final error equation is obtained.

$$error = \sqrt{\left(\frac{60\frac{s}{min}}{t}\right)^2 d_{err}^2 + \left(-\frac{\left(60\frac{s}{min}\right)\cdot d}{t^2}\right)^2 t_{err}^2} \tag{B.5}$$

APPENDIX C: STANDARD OPERATING PROCEDURE

This document is intended to give instructions to run the MHD micropump, provided the pieces have already been fabricated.

1. Prepare solutions. Typically, a trial is run with a colorless solution in the channel and a dyed solution on the inlet port, both with the same concentration of NaCl. Start with 0.02 g of erioglaucine disodium salt per 10 mL of water for the dyed solution. This concentration makes the dye visible in the channel. Any lower and the dye is difficult to see. Typical NaCl concentrations are 0.01 M to 1 M. Be sure not to exceed the solubility limit of NaCl, as solid crystals will not pass through the channel.
2. UNPLUG THE ARDUINO FROM THE POWER SOURCE. Ensure the Arduino Microcontroller is properly wired. The button should be connected to pin 13 through a 330 Ω resistor and the device electrodes should be connected to pin 3 and ground. The positive electrode should also be connected to pin 0 for the current flow check.

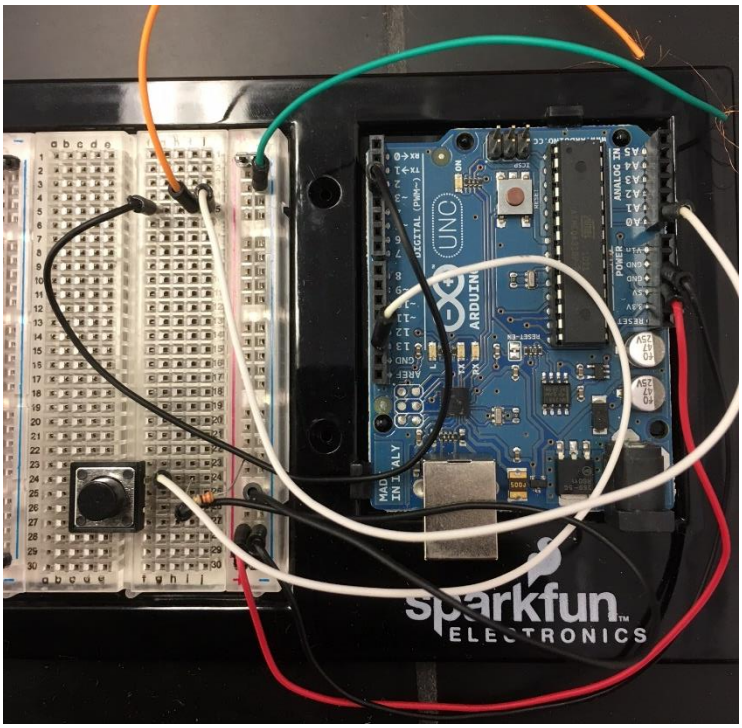

3. Ensure the Arduino code editing software is running on the computer. It is available for free download at https://www.arduino.cc/en/Guide/HomePage, or you can use the web editor.
4. Plug the Arduino into the computer running the code. It may take the computer a couple of minutes to recognize and connect the Arduino, especially the first time it is plugged in on a given computer. Troubleshooting guides are available online if the Arduino software does not recognize the hardware. To check if the device is fully connected, click on "Tools." If "Port" is clickable and at least one option is listed, the Arduino is connected. The image below shows "Port" greyed out in the event no Arduino is connected.

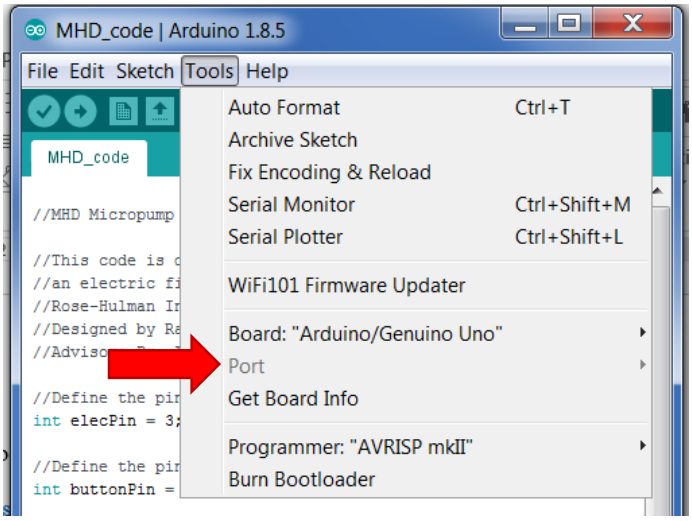

5. Set the PWM value for the desired duty cycle. This is the line: analogWrite(elecPin, ###). 255, 100%. 191, 75%.127, 50%. 64, 25%.

6. Upload the code to the device. This also saves the code to the computer with any changes that have been made.

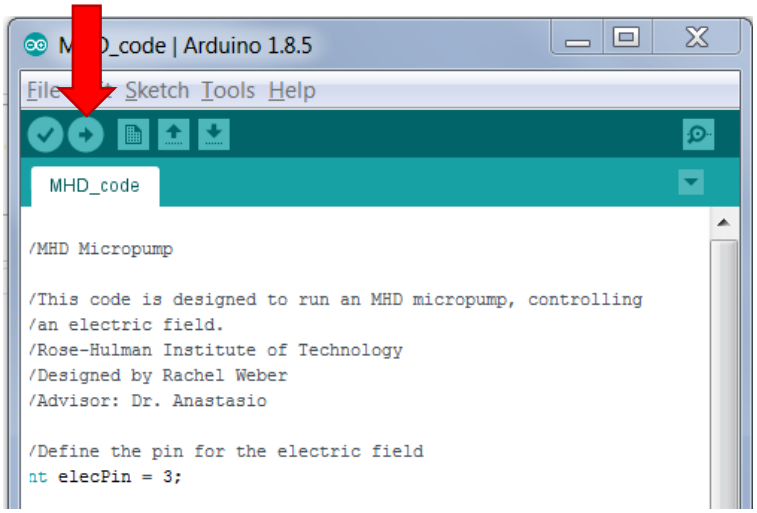

7. Open the serial port. The scrolling numbers should be 0 when the button is not pushed, and the device is not running; they should be nonzero when the button is pushed, and current is flowing through the device. Repeated testing has shown a value of 1023 when running the device. The frequency of the 1023 output vs. the 0 output is dependent on the duty cycle.

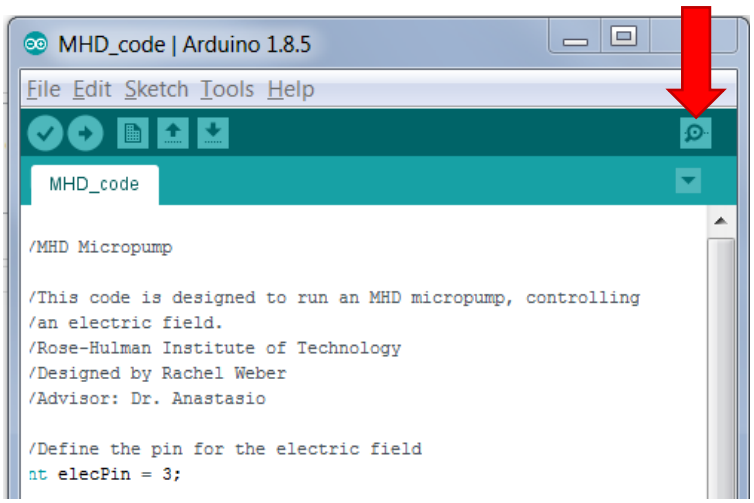

8. Align the PDMS channel on the electrodes. Though difficult to see in the image, you should be able to visually ensure the electrodes will both contact the fluid for the entire length of the channel.

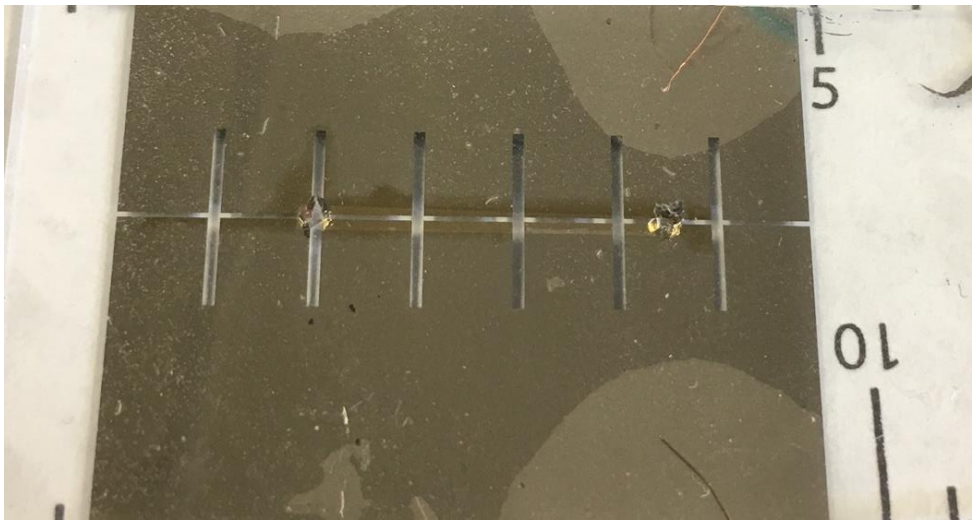

9. Use your fingers to squeeze the PDMS and the glass together, removing any air bubbles.
10. Lift the side of the PDMS to insert each wire, then squeeze the PDMS onto the wire. Ensure the air pocket caused by the wire does not reach the channel.

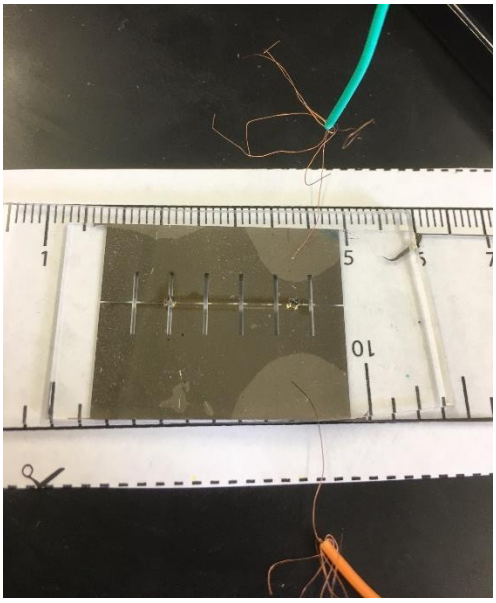

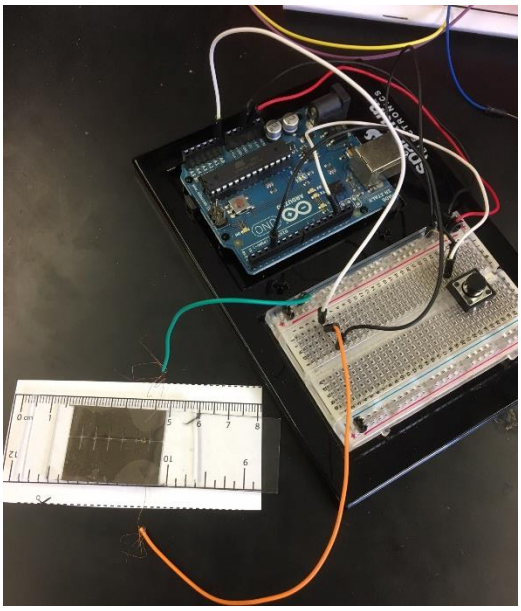

11. CAREFULLY lift the glass slide and place it on top of the printed ruler and permanent magnet.

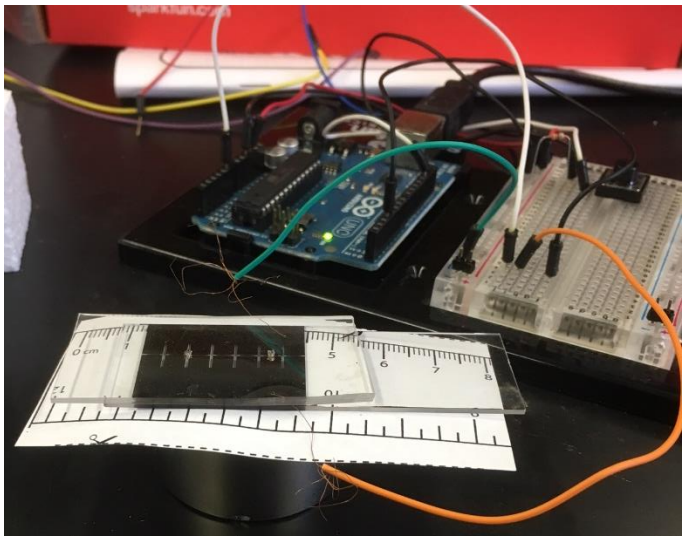

12. Using the flat fronted syringe, draw up the colorless solution. Place the flat front of the syringe all the way to the bottom of the inlet port and squeeze SLOWLY. Liquid will bead on the surface of the PDMS, but should also flow through the channel. You may need to adjust the angle of the syringe to get the liquid to flow through the channel. Watch the outlet port and squeeze until liquid has filled the entire channel and is beading on the outlet port.
13. Clean the bead of liquid off the inlet port.
14. Clean the syringe.
15. Place a device capable of recording video above the channel. Ring stands are useful for hands-free recording.
16. Adjust the channel so that the millimeter gradations on the ruler are visible through the channel and on the video camera.

17. Using the flat fronted syringe, place a bead of the dyed solution on the inlet port. The image below was taken with the same device that was used to record trials, and is a good example of what the video should look like.

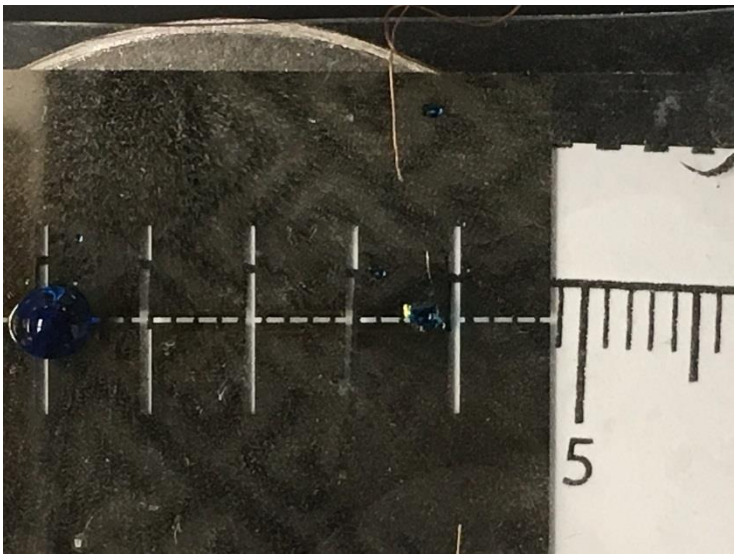

18. Press and hold the pushbutton on the breadboard. Watch the serial port to ensure current is flowing.
19. Wait for the dyed solution to enter the channel. This can take up to five minutes.
20. Press record on the video camera.
21. Wait for dye to travel through the entire channel. The farther the dye travels, the more accurate the final velocity calculation will be.
22. Let go of the pushbutton and stop the video camera.
23. Slide the wires out of the device.
24. Peel the PDMS off the glass slide and clean both thoroughly. Erioglaucine disodium salt should not go down the drain.

25. Set the glass slide and the PDMS channel side up on a paper towel to air dry. Paper gives off a large number of particles, which make it difficult for the PDMS to stick to the glass. Do not use the paper towel to directly dry the components.